Yang *et al. Biochar* (2022) 4:51
https://doi.org/10.1007/s42773-022-00169-8

Biochar

REVIEW Open Access

Advances in preparation, application in contaminant removal, and environmental risks of biochar-based catalysts: a review

Bowen Yang[1], Jiawei Dai[1], Yuan Zhao[2], Jingwei Wu[1], Caiya Ji[2] and Yuhu Zhang[1*]

Abstract

As a carbon-rich material produced by pyrolysis of biomass, biochar features low cost, large specific surface area, and widely available feedstocks based on the functional diversity and environmental-friendly properties, it has received increasing attention in the fields of pollutant removal due to three win–win effects of water remediation, carbon sequestration and reutilization of wastes. To design excellent biochar-based catalysts for environmental applications, one must understand recent advances in the catalysts for contaminant removal. This review focuses on the current application of biochar-based catalysts in redox systems, Fenton-like systems, sonocatalytic systems and photocatalytic systems. Besides in-depth discussion in effects of preparation conditions on physicochemical characteristics of biochars, the review supplements new preparation technologies of biochar and biochar-based catalysts. Most importantly, the advantages/shortcomings, catalysis mechanisms, as well as the pollutant removal ability of different types of biochar-based catalysts are discussed. The environmental risks of the catalyst applications are also elaborated on. Future research on biochar-based catalyst production and its environmental applications is discussed. The review provides a good overview of the current advances of biochar-based catalysts in pollutant control and the future research directions.

Article Highlights

- Biomass type and thermochemical conversion temperature significantly affect biochar physicochemical properties.
- Biochar-based catalysts applied in Fenton-like system exhibited better performance for refractory emerging pollutants.
- Biochar-matrix, metal nanoparticles of catalysts, as well as intermediates are the main risks.

Keywords: Biochar-based catalysts, Sonocatalysts, Fenton-like catalysts, Photocatalysts, Pollutant removal, Environmental risks

*Correspondence: yuhu.zhang@cnu.edu.cn

[1] College of Resource Environment and Tourism, Capital Normal University, Beijing 100048, China
Full list of author information is available at the end of the article

Graphical Abstract

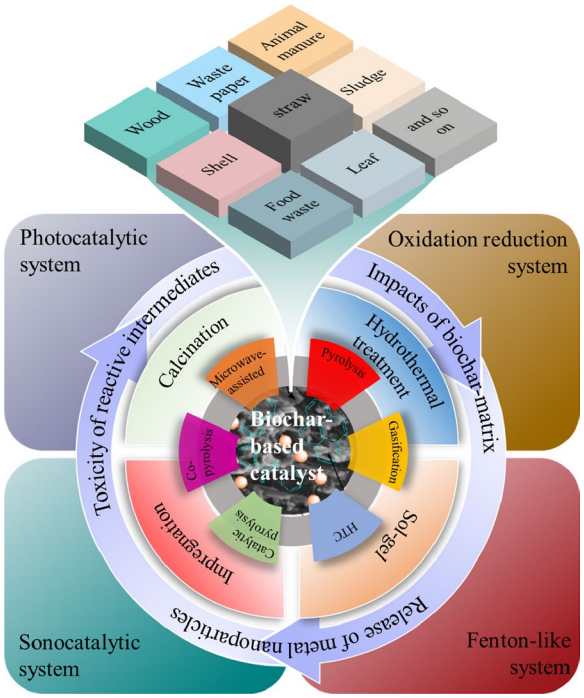

1 Introduction

Nowadays, with the development of industrialization and urbanization, various contaminants, including heavy metals, antibiotics, polychlorinated biphenyls, pesticides, endocrine disruptors, volatile organic compounds, and polycyclic aromatic hydrocarbons are released into the air, water and soil environment (Kwon et al. 2020; Lu et al. 2020). These pollutants could pose a serious threat to the ecosystem and public health. Various green remediation technologies have been developed for the removal of these pollutants from the environment. Based on the concept of green restoration, biochar (BC), as a promising multifunctional porous carbon material, has gathered much more attention (Wang et al. 2019a). The abundant feedstocks, huge specific surface area, abundant functional groups, porous structure, and low cost endow biochar with enormous potential for application in the field of pollutant remediation (Issaka et al. 2022; Liang et al. 2021), energy shortage (Bolan et al. 2022; Chen et al. 2019b) and climate change reversal (Tam et al. 2020).

Biochar is a porous carbonaceous product obtained from the thermochemical decomposition of biomass under an oxygen-limited atmosphere (Aller 2016). Almost all biomass, including organic municipal solid wastes, food wastes, agricultural residues, sewage sludges, manures, algas, wood chips and so on, can be used to produce biochars (Lopes and Astruc 2021; Shaheen et al. 2019). Besides feedstock, the physicochemical properties of biochars are largely determined by thermochemical decomposition conditions including temperature, residence time and heating rate (Xiang et al. 2020; Zhao et al. 2018). Whereas the adsorption process could not completely decontaminate contaminants, compared to adsorption, catalysis technology can eliminate contamination by redox reaction. Recently, increasing attention has been paid to the applications of biochars in the field of pollutant catalytic oxidation–reduction (Fang et al. 2017; Lyu et al. 2020; Wang et al. 2019a). Easily tunable functional groups, chemical stability and electrical conductivity also make biochars act as a platform for supporting various catalytic nanoparticles (Ahmaruzzaman 2021; Kwon et al. 2018). The biochars with excellent electron-conductivity contribute to electron transfer, which reduce the recombination of the e^-/h^+ pair of semiconductor photocatalysts (Zhai et al. 2020). Moreover, the incorporation of biochar can modify the weak visible light sensitivity, low adsorption capacity and easy agglomeration of the photocatalysts (Ye et al. 2019). Besides photocatalytic system, many researchers used biochar-based catalysts for peroxide activation to

induce the generation of reactive oxygen species (ROS) (Gholami et al. 2020b; Liu et al. 2020c; Luo et al. 2021; Wang et al. 2022). However, some defects such as light dissolution and harmful metal ions release limited the larger-scale application of these catalysts. Based on the special surface structure and redox-active moieties (Chen et al. 2015, 2017; Fang et al. 2015, 2017; Li et al. 2020; Liu et al. 2019b), such as oxygen functional groups (OFGs), mineral components, dissolved organic matter (DOM) and persistent free radicals (PFRs), attentions have been paid to direct generation of ROS for the degradation of contaminants by using biochar-based catalysts (El-Naggar et al. 2020; Wu et al. 2021).

Few reviews have systematically reviewed the advance of biochar-based catalysts for the removal of contaminants. Consequently, the overarching objective of this work is to present a comprehensive review on the applications of biochar catalytic technology in pollutant control. Besides the detailed description of conventional preparation methods of biochar, the review supplements new technologies on the preparation of biochar and biochar-based catalysts, and the correlation of biochar properties with catalysis. Comparatively, the two parts of the content are important but were overlooked in the previous review. After that, this review digests current applications of biochar-based catalysts in redox, Fenton-like, sonocatalytic, and photocatalytic systems. Most importantly, the advantages/shortcomings, catalysis mechanisms, as well as the pollutant removal ability of different types of biochar-based catalysts are discussed. Moreover, as an environmental function material, eco-friendly is an extremely important property to evaluate, hence the environmental risks of the catalyst applications are also elaborated. Finally, the perspectives and future research directions of biochar-based catalysts are discussed.

2 Recent progress of biochar production technologies

Biochar, is the precursor of biochar-based catalysts, and its synthesis and properties greatly affect the catalysis performance of catalysts. Nowadays, conventional pyrolysis methods are widely used to prepare biochars, and emerging advanced pyrolysis techniques are developing boomingly. The yield, surface area, pH, ash, and fixed carbon, volatile matter, polarity and aromaticity with their according pyrolysis temperatures are important to design useful biochar catalysts as they indicate the success of the pyrolysis process. Therefore, the relationship between preparation conditions and performance of materials should be taken into consideration. Table 1 summarizes different technologies for the preparation of biochars with advantages and shortcomings.

2.1 Conventional production technologies

The biochar conventional production technologies include pyrolysis, gasification and hydrothermal carbonization. Recently, the conventional pyrolysis and hydrothermal carbonization are still the most widely used methods to prepare biochars.

2.1.1 Pyrolysis

In general, pyrolysis proceeds under oxygen-free conditions at temperatures ranging from 300 to 900 °C. Figure 1 shows the effects of temperature on properties of biochars. The most rapid decrease in yield occurs at 200–400 °C, and yields at least 30% could be obtained under 800 °C. It could be found that the pH increased with increasing temperature due to the detachment of the acidic functional groups, which led to an increase in alkalinity. Additionally, the relative content of the ash and the surface area follow the same rule (Weber and Quicker 2018), but it is not possible to estimate the surface area based on the temperature alone, and the surface area may decrease after a further increase of temperature (Weber and Quicker 2018). Figure 1e shows the decrease rate of O/C ratios is higher than that ofH/C ratios with the increase in temperature, indicating decreased polarity and increased aromaticity. Obviously, the decrease in atomic ratios does not occur linearly with the pyrolysis temperature. Figure 1d shows that the biochar transformed from volatile matter to fixed C as temperature increased. Besides, a longer residence time can increase biochar yield and fixed carbon content due to the repolymerization of char constituents and decrease the volatile matter content, at the same pyrolysis temperature (Zhao et al. 2018). The surface area and morphology are more significantly influenced by residence time, which is often overlooked in previous literature (Zhao et al. 2018).

2.1.2 Gasification

Gasification could produce syngas, tars and char via the gaseous media (nitrogen, air, oxygen, steam etc.) to partially oxidize the feedstock, hence, it requires high temperatures ranging from 700 to 900 °C (Tam et al. 2020). The low O/C ratio of feedstock used in this process usually leads to efficient gasification (Kim et al. 2020). Similarly, the product depends on the reaction temperature, pressure, and temperature rising rate. The temperature is the most important parameter directly affecting the gasification reactions, and a higher temperature can increase the yield of H_2 and CO, carbon conversion and cold gas efficiency, while reducing the contents of CO_2, CH_4, hydrocarbons and tar contents (Cha et al. 2016; Han and Kim 2008; Taba et al. 2012). In addition, the types of gasification agents significantly affect the characteristics of the biochar. It was reported

Table 1 Technologies for production of biochars with advantages and shortcomings

Method of preparation	Preparation temperature	Retention time	Biochar yield	Advantages	Shortcomings	References
Pyrolysis	300–900°C	Minutes to days	30–60%	Simple and direct technology, low cost, porous structure, high S_{BET}	Reduced acidic functional groups, low adsorption capacity due to the partial oxidation of feedstock, poor properties	Jiao et al. (2021)
Gasification	700–900°C	10–20 s	10–20%	Low residence time and cost, high gas yield	High temperature, less quantity of biochar as a by-product, the generation of greenhouse gases	Murtaza et al. (2021)
Hydrothermal carbonization	180–350°C	1–12 h	60–90%	Easy to decompose biomass in an aqueous medium, no need to dry biomass, convenient for coating pre-formed nanostructures with carbonaceous shells	The feedstock limited by simple carbohydrates	Cheng and Li (2018)
Catalytic pyrolysis	300–600°C	Minutes to hours	40–60%	Low temperature due to catalysts, high yield, improved product quality	Contamination caused by catalysts	Sekar et al. (2021)
Co-pyrolysis	250–600°C	Several hours	30–60%	The thermal degradation of a mixture of two or more biomass feedstocks develops multiple properties of biochars through synergistic effects	Same with pyrolysis	Fakayode et al. (2020)
Microwave-assisted pyrolysis	300–700°C	Hours to days	20–50%	Uniform heating, high power conversion efficiency, low thermal inertia, reduced energy consumption	Restrictions on the reaction conditions, the power and life of the magnetron, microwave leakage	Zhang et al. (2022)
Calcination	300–700°C	Several hours	30–60%	Two or multifarious solid phase matters are closely bound together	High calcination temperature destroys the structure of biochar and decreases S_{BET}	Baig et al. (2016)
Hydrothermal treatment	90–220°C	2–24 h	–	More OFGs, high S_{BET} and V_t, mild safety conditions	Poor stability, secondary pollution	Wang et al. (2020d)
Sol–gel	Water bath heating	Hours to days	–	Easy to uniformly and quantitatively incorporate some elements to improve performance, easy reaction process, low temperature	High cost of raw metal alkoxide, toxic organic solvents, long process, volatile gas	Xie et al. (2019)
Impregnation	–	Hours to days	–	Simple operation, good stability, less metal leaching	Secondary pollution	Panwar and Pawar (2022)

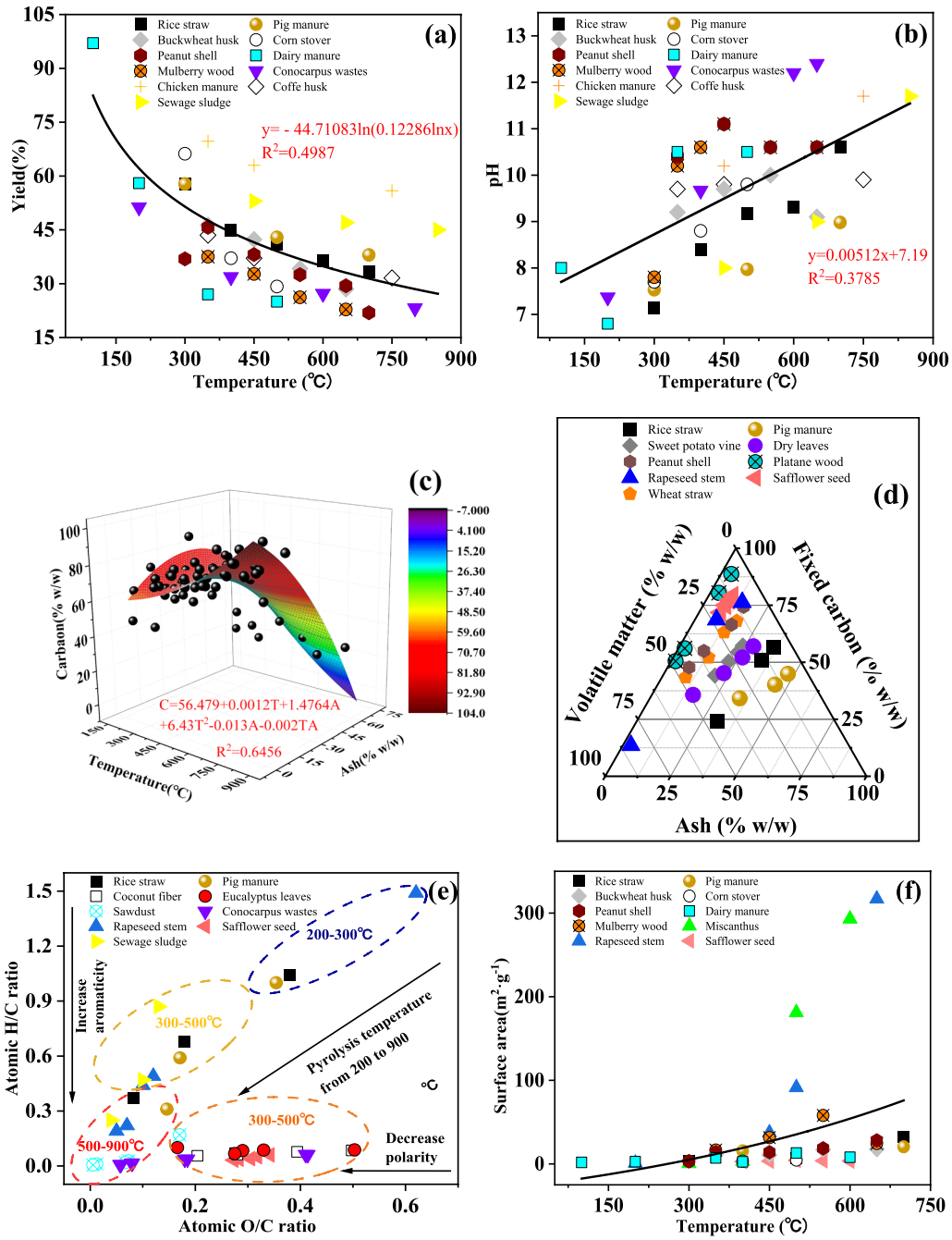

Fig. 1 Percent yields (**a**), pH (**b**), Van Krevelen diagram (**e**), surface area (**f**) of biochar from different feedstocks at different pyrolysis temperatures; Biochar total carbon content (% w/w) changes with peak pyrolysis temperature and ash content (**c**); Biochar ash, volatile matter, and fixed carbon proportions expressed as weight % in a ternary graph for each biochar type (**d**). [Data are from reference (Cha et al. 2016; Chandra and Bhattacharya 2019; Das et al. 2021; Liu et al. 2017b; Sun et al. 2017; Tomczyk et al. 2020; Xie et al. 2015; Zhao et al. 2018)]

that the ratio of the aromatic ring structure of the aromatic compounds composing the char was lower and the contents of alkaline metals, such as Mg and Ca, were higher when H_2O was used, the presence of steam could accumulate radicals on the char surface, forming some additional structures (such as hydroxides or oxides), which prohibited the formation of carbonates or their agglomerates (Tay et al. 2013).

2.1.3 Hydrothermal carbonization

Hydrothermal carbonization (HTC) based on the reaction medium of water at relatively lower temperatures and higher pressures can convert biomass with moisture content into biochar with higher carbon content (Gale et al. 2021). In HTC process, the biomass needs not to achieve the drying step, and the product yield is higher (up to 88%) than that from pyrolysis and gasification (less than 60%), hence HTC is more energy efficient to obtain the same quality biochars (Cha et al. 2016; Meyer et al. 2011; Parmar et al. 2014). The effects of the temperature on properties of hydrochar are shown in Fig. 2. In HTC process, the hydrochar products are usually generated below 250 °C (Fernandez-Sanroman et al. 2021), and temperature is a vital factor, which initiates an ionic reaction in the subcritical regions (Khan et al. 2019). In terms of pH, even with an increasing trend along with temperature, hydrochars exhibited slightly acidic or mildly basic with pH-values ranging between 6 and 8 due to the formation of organic acids during the hydrothermal process, which is different significantly from pyrolysis biochars (Vassilev et al. 2010). The proximate analysis indicated hydrochars have higher volatile matter content while lower ash content than pyrolysis biochars. Carbon content (C) correlates well with the ash content (A) and pyrolysis temperature (T) ($R^2 = 0.9447$, Fig. 2c), so it is possible to accurately prepare hydrochars with desirable carbon and ash content by adjusting the hydrothermal temperature. Figure 2e indicates that an increase in hydrothermal temperature instigates a reduction in H/C and O/C ratios, resulting from the degree of the condensation reaction (Sevilla and Fuertes 2009). Note that the decrease in atomic ratios occurs linearly with pyrolysis temperature ($R^2 = 0.9022$, Fig. 2e), proposing an estimation of atomic ratios based on the temperature alone could be possible.

2.2 Advanced pyrolysis techniques

Conventional pyrolysis may not be promising for the development of multiple properties of biochars. Based on the shortcomings of conventional techniques, advanced pyrolysis methods are developed to improve the yields, qualities, characteristics and properties of products. Currently, advanced pyrolysis techniques involve several approaches, including catalytic pyrolysis, co-pyrolysis, microwave-assisted pyrolysis and combination of multiple technologies.

2.2.1 Catalytic pyrolysis

Catalytic pyrolysis is usually used to prepare high value-added chemical energy products. The use of proper catalysts can improve the pyrolysis process and characteristics of the products. Biochar materials can be used as promising catalysts. For example, a previous study showed that the co-production of bio-oil and MgO-impregnated biochar from catalytic pyrolysis of Mg-loaded biomass favored the thermal degradation process due to the weakened hydrogen-bonding networks and disrupted the crystalline structures. The relative contents of ketones and furans increased, and the relative contents of phenols and sugars decreased for Mg-loaded samples (Zhang et al. 2020c). Therefore, the use of catalysts is relatively promising due to lower energy requirement, pyrolysis temperature and enhancement of product selectivity (Lee et al. 2020). Because some catalysts may be expensive, poisoned or ineffective, a proper selection of catalysts is extremely necessary during the process of catalytic pyrolysis (Gholizadeh et al. 2021; Kabir and Hameed 2017; Zheng et al. 2017). It was noted that although the derived cobalt-impregnated biochar exerted excellent catalytic activity to activate peroxymonosulfate (PMS) for atrazine degradation, all transformation by-products and parent atrazine were still classified as very toxic compounds to aquatic organisms (Liu et al. 2020a). Fredriksson used olivine as an active bed material for catalytic cracking of tars during gasification of biomass, the carbon deposition observed after exposing olivine to reducing conditions can result in significant catalyst deactivation (Fredriksson et al. 2013).

2.2.2 Co-pyrolysis

Compared to conventional pyrolysis, co-pyrolysis is a process that entails the thermal degradation of a mixture of two or more biomass feedstocks through the generation of synergistic effects, hence it could improve the pyrolysis method for the development of multiple properties of biochar used in applications (Ahmed and Hameed 2020). Depending on the synergistic effects and interactions of multifarious biomass materials, co-pyrolysis can significantly improve the quality of the product. Many studies indicated that the yield of biochar, pore structure, ash content, and heating value would have an improvement by co-pyrolysis (Fakayode et al. 2020; Li et al. 2021). It demonstrated that the surface area and higher heating value of biochar derived from co-pyrolysis of rice husk-pine sawdust and seaweed are 3.83 and 1.16 times higher than those of seaweed-derived biochar (De Bhowmick et al. 2018). Some studies also indicated that co-pyrolysis could enhance adsorption performance toward a variety of pollutants. Kwon reported that Cu(II) adsorption capacity of co-pyrolysis biochar derived from chitin and oyster shell had a promotion and synergistic effects enhanced the properties of biochar (Kwon et al. 2022). A review summarized that merging lignocellulosic and macroalgae biomass feedstocks can be successfully employed for biochar production in the energy

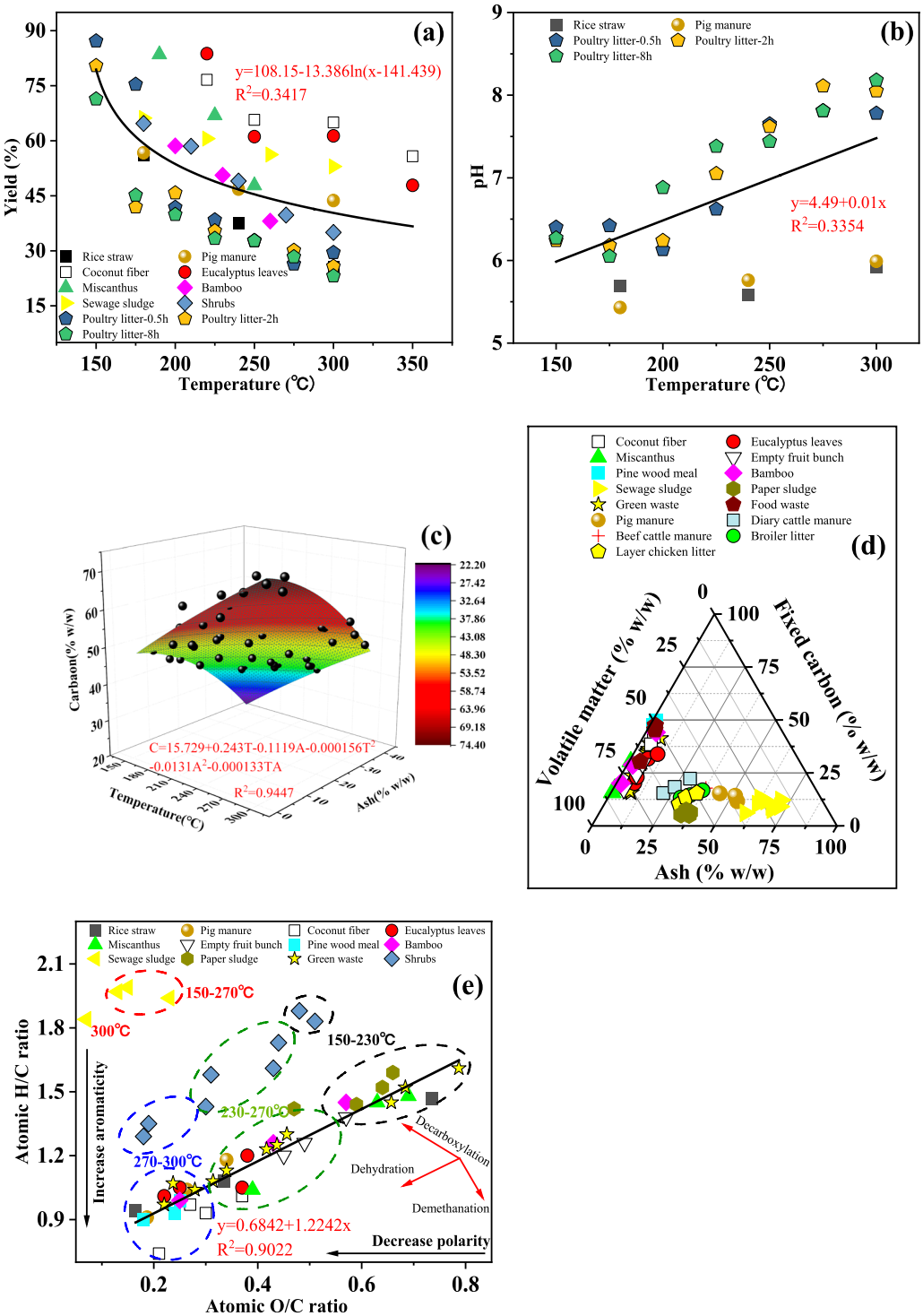

Fig. 2 Percent yields (**a**), pH (**b**), Van Krevelen diagram (**e**) of hydrochar from different feedstocks at different pyrolysis temperatures; Hydrochar total carbon content (% w/w) changes with peak pyrolysis temperature and ash content (**c**); Hydrochar ash, volatile matter, and fixed carbon proportions expressed as weight % in a ternary graph for each biochar type (**d**). [Data are from reference (Ghanim et al. 2016; Liu et al. 2017b; Raheem et al. 2022; Saqib et al. 2018; Wang et al. 2018c; Yao et al. 2016; Zhang et al. 2020b; Zhou et al. 2019; Zhu et al. 2015)]

biorefinery (Fakayode et al. 2020). While co-pyrolysis is a developing technology that is being keenly explored at present, more considerable attention, such as temperature, heating rates and feedstock types and blending ratio, pretreatment and economic analysis should be given to it considering the various benefits derived from its utilization (Fakayode et al. 2020).

2.2.3 Microwave-assisted pyrolysis

Microwave-assisted pyrolysis has boomed over the past 5 years (Lee et al. 2020). In microwave pyrolysis of biomass, the heat transfer is more efficient as the heat is generated within the core of material by the interaction of microwaves with biomass (Foong et al. 2020), hence leading to energy saving. The microwave power and interaction of heating time and microwave power positively affected the maximum yield of biochar (Sahoo and Remya 2020). The pyrolysis heating rate greatly depends on the temperature, power of the microwave, microwave absorb ability and pyrolysis feedstock (Lee et al. 2020). The induction of additives, such as the absorber or catalysts, can further promote microwave-assisted pyrolysis, and the properties of biochars obtained through microwave pyrolysis are significantly different from those of conventional pyrolysis. Biochar is also an excellent additive for biomass pyrolysis due to its high microwave absorbability (Wang et al. 2020a). In a previous study (Haeldermans et al. 2019), an increasing microwave power without the use of absorbers led to a higher degree of aromaticity and a more open surface of biochar (Jiao et al. 2021). The microwave-assisted pyrolysis can be considered as a new form of development, however, the lack of excellent reactor design can be a main obstacle that impedes the commercialization of biomass recycling (Foong et al. 2020).

2.3 Cost factor

The cost is a non-negligible factor when preparing biochars. Pyrolysis is a so important technology in the biomass energy industry development with simplicity in design and operation. More importantly, it allows to input almost all types of biomasses at various sizes (Low and Yee 2021). Many researches have investigated the cost of pyrolysis. Jenny found that the conventional pyrolysis of biochar and methanol yields the minimum carbon price of $642.40 per Mg, while fast pyrolysis biochars achieve the minimum carbon price of $61.38 per Mg (Meyer et al. 2011; Raheem et al. 2022), but researchers should make a promotion on the property and yield of biochar by pyrolysis to improve this method. Catalytic pyrolysis could reduce the production cost by reducing energy input. The introduction of catalysts could obtain the product with higher yields and better quality at lower temperatures. Nevertheless, the cost of catalysts should be taken into consideration and most of the studies regarding catalytic pyrolysis are still in the lab scale, and attention should be paid to this aspect in future studies (Yang et al. 2022). Gasification is often performed at large scales thus producing several tons of biochar per day as a co-product. The cost of $380 per ton and large volumes of gas make gasification an incidental method to produce biochars, and interestingly, it was found a higher heating value of 18.9 MJ for gasification biochars (Low and Yee 2021; Meyer et al. 2011; Norgate and Langberg 2009). However, the cost will increase greatly if biomass moisture content is high. HTC is a suitable method that could convert biomass with any moisture content into biochars with higher carbon content, and it was reported that the yield could reach 20 kilotons per year with $190.15 per ton production cost by HTC (Nizamuddin et al. 2017; Pacheco Antero et al. 2020). Microwave-assisted pyrolysis is another method to handle biomass with high moisture content, and the water in biomass has been shown to increase the rate in a microwave pyrolysis reactor, thereby increasing the heating efficiency (Hadiya et al. 2022). Therefore, the microwave pyrolysis of biomass is profitable when biochar pyrolysis oil and non-condensable gas are considered. Co-pyrolysis is similar to pyrolysis on economic feasibility, and the difference lies in the selection of raw materials, but rare references investigated the co-pyrolysis costs. Note that the high value applications of the remaining co-pyrolysis products will greatly improve the economics of biochar production (Fakayode et al. 2020).

3 Recent progress of biochar-based catalyst synthesis

Several approaches have been developed for biochar-based catalyst synthesis from different feedstocks. Among them, calcination, hydrothermal treatment, sol–gel, and impregnation are by far the most important technologies (Table 2).

3.1 Calcination

Calcination usually proceeds under N_2 or air conditions at temperatures ranging from 300 to 700 °C, which is similar to pyrolysis. Calcination is one of the most common methods for preparing biochar based-catalysts, by which two or multifarious solid phase matters are closely bound together to achieve composite multi-functionalization. Compared with pyrolysis, calcination could increase the hardness of materials, prevent their breakage, and change material textural and mineralogical characteristics (Baig et al. 2016). Just as its name implies, the temperature, gas phase composition, and thermal stability of the compound significantly affect the calcination process. A series of TiO_2/pBC composites were prepared

Table 2 Synthesis parameters and characteristics of various biochar-based catalysts

Biomass types	Preparation methods	Preparation conditions	Catalysts	Characteristics					Active moiety	References
				C (wt %)	O (wt %)	Metal (wt %)	BET ($m^2 \cdot g^{-1}$)	V_t ($cm^3 \cdot g^{-1}$)		
Pine needles	Pyrolysis	300°C; 10°C·min^{-1}; 6 h	Pine needle biochar	65.1	26.2	–	5.24	–	OFGs; [FRs] = 5.38 × 10^{18} spins·g^{-1}; [·OH] = 75 μM	Fang et al. (2015)
Cotton straw	Pyrolysis; activation	350°C; 10°C·min^{-1}; 2 h; NH_2Cl treatment	Cotton straw biochar	–	–	–	39.005	0.03514	N, Si elements; [FRs] = 8.25 × 10^{16} spins·g^{-1}	Wang et al. (2019c)
Red mud and lignin	Pyrolysis	700°C; 10°C·min^{-1}; 1 h; N_2 flow rate 500 mL·min^{-1}	Mixed metal-biochar composites	32.0	35.0	27.2	100.8	–	Metal oxides; metallic Fe	Cho et al. (2019)
Fir sawdust	Adsorption; fast pyrolysis	773 K; N_2	Ag@biochar	86.2	10.7	1.1	27.8	–	Ag NPs	Liu et al. (2016)
Rice straw	Impregnation; pyrolysis	Salt solution impregnation; 800°C for 4 h; 5°C·min^{-1}	N-biochar @ $CoFe_2O_4$	76.4	20.2	–	150.7	0.081	Hydroxyl groups; Co^{3+}; phenolic and quinone moieties; graphitic N	Liu et al. (2019a)
Camellia seed husks	Impregnation; pyrolysis; co-precipitation	400°C for 2 h; HNO_3(68%) + H_2SO_4 (70%) soaking 1 h	oxidation biochar-Fe_3O_4	29	36.8	31.29	–	–	OFGs; Fe_3O_4 particles; carbon hybridization; defective sites; PFRs	Pi et al. (2019)
Wheat husks, paper sludge	Pyrolysis; impregnation; hydrothermal treatment	BC: pyrolysis at 500°C for 20 min; $Zn(NO_3)_2$ solution; hydrothermal: 90°C for 2 h	ZnO-biochar	26.15	35.93	31.09	119.15	0.16	Functional groups; porous particles; ZnO; metals like Si and Al that exist in biochar gallery	Gholami et al. (2019a)
Biochar	Oxidation; hydrothermal method	Oxidation by H_2SO_4, HNO_3; hydrothermal method at 90°C for 24 h	Fe-Cu-LDH / biochar	28.93	6.32	64.75	91.35	0.89	Fe-Cu LDH	Gholami et al. (2020a)
Platanus orientalis linn branches	Sonication; pyrolysis	650°C for 2 h; sonication with $FeCl_3$ at 25°C for 1 h; 650°C for 1 h	FeBC	81.86	3.31	7.34	–	–	Fe-loaded biochar could increase the immobilization of potentially toxic elements through (co)precipitation	Wen et al. (2021)
Paper waste, wheat straw	Pyrolysis; hydrothermal method; calcine	500°C for 20 min; 90°C for 24 h; 500°C for 2 h with air	CeO_2H@biochar	23.67	31.28	36.6	59	0.19	Biochar trap electrons in CB of CeO_2; metals in the BC galleries act as π acceptor metals	Khataee et al. (2018)

Table 2 (continued)

Biomass types	Preparation methods	Preparation conditions	Catalysts	Characteristics					Active moiety	References
				C (wt %)	O (wt %)	Metal (wt %)	BET ($m^2 \cdot g^{-1}$)	V_t ($cm^3 \cdot g^{-1}$)		
Pine pollen	Hydrothermal; in-situ precipitation	180°C for 12 h	biochar@ $CoFe_2O_4/Ag_3PO_4$	–	–	–	21.848	0.059	Biochars assist e^- to move; Z-scheme heterojunction between MB and Ag_3PO_4	Zhai et al. (2020)
Glucose	Hydrothermal; activation	180°C for 10 h; 600°C for 90 min	Fe_3O_4 hydrochar	–	–	9.17	1072	0.3979	Fe(II); magnetic hydrochar	Wang et al. (2020d)
Hog fuel, demolition waste	Pyrolysis; hydrothermal	600°C for 30 min; 180°C for 3 h	Cu_2O-CuO @ biochar	18.19	44.17	37.64	32.91	0.37	Biochar; Cu_2O-CuO	Khataee et al. (2019)
Hemp stems	Sol–gel; calcine	500°C for 2 h in N_2	TiO_2-CuO/HSC	–	–	–	17.35	0.064	HSC; CuO; TiO_2	Peng et al. (2019)
Wheat husks, paper sludge	Pyrolysis; modification; hydrothermal	500°C for 20 min; $H_2SO_4 + HNO_3$; 90°C for 24 h	Zn-Co LDH-@ biochar	21.73	30.16	37.26	95.76	0.11	Zn—Co—LDH; biochar	Gholami et al. (2020b)
Walnut shells	Pyrolysis; hydrolysis	500–800°C for 2 h; calcined at 500°C for 1 h	TiO_2/biochar	11.7	86.92	–	–	–	Biochar transfer electrons and acted as acceptor	Lu et al. (2019)
Reed straw	Pyrolysis; sol–gel	500°C for 6 h	TiO_2/pBC	–	–	–	102.160	0.0122	TiO_2	Zhang et al. (2017)
Activated carbon	Sol–gel; calcine	80°C for 4 h; 500°C for 2 h	AC-TiO_2	47.7	30.2	22.1	360.4	0.0348	Lignocellulosic materials collect and transfer electron–hole charges; C=O and O=C–OH as electron acceptor	Djellabi et al. (2019b)
Olive pits			OP-TiO_2	23.1	39.1	37.8	55.13	0.0147		
Wood shaving			WS-TiO_2	31.4	35.7	32.9	30.04	0.0147		
Chicken feather	Hydrothermal cross-link	Air dry at 200/220°C for 8 h; argon at 450°C for 1 h	TINCs	75.14	15.14	5.91	64.10	–	Ti–O–C; Ti–O–Ti and Ti-N bonds	Li et al. (2018)
Reed straw	Pyrolysis; sol–gel; calcined	500°C for 6 h; 300°C for 2 h	Zn-TiO_2/biochar	40.44	31.31	26.78	169.158	0.0159	Zn; TiO_2	Xie et al. (2019)
Olive pits	Sol–gel; hydrothermal; magnetization	500°C; 180°C for 6 h	TiO_2-OP @Fe_3O_4	–	–	–	104.7	0.175	Ti–O–C bridge; OP act as a photosensitizer for TiO_2 or electrons acceptor	Djellabi et al. (2019a)
Sewage sludge	Impregnation; thermal decomposition	800°C for 1 h; $10°C \cdot min^{-1}$ under N_2	TiO_2/Fe/Fe_3C-biochar	–	–	–	267.3	0.33	Mesoporous surface; Ti^{3+}; Fe_3C and Fe^0	Mian and Liu (2019)

Table 2 (continued)

Biomass types	Preparation methods	Preparation conditions	Catalysts	Characteristics					Active moiety	References
				C (wt %)	O (wt %)	Metal (wt %)	BET ($m^2 \cdot g^{-1}$)	V_t ($cm^3 \cdot g^{-1}$)		
Chestnut leaves	Pyrolysis; thermal poly-condensation	900°C for 2 h; 300°C for 2 h; 520°C for 2 h	g-C_3N_4 modified biochar	61.2	–	38.8 (N)	8.05	–	Biochar mainly acts as adsorbent; electron-transfer channels and acceptors	Pi et al. (2015)
Bamboo	Hydrothermal; calcine; impregnation	180–200°C; 550°C for 4 h; 70°C for 60 min	Biochar@g-C_3N_4 core–shell catalysts	–	–	–	34	–	Biochar spheres acted both as a reservoir and sensitizer	Wang et al. (2018b)
α-D-glucose	One-pot HTC	180°C for 12 h	Fe_3O_4/C/g-C_3N_4	–	–	–	79.9	–	Carbon and Fe_3O_4 with superior electron transfer ability	Ding et al. (2018)
Biochar	Hydrolysis method	Room temperature for 12 h	Biochar/BiOX (X = Br, Cl)	–	–	–	–	–	Biochar acted as an electron reservoir	Li et al. (2016)
Lotus-leaf	Calcinate	300°C for 1 h; N_2	CdS@LAC-800	39.0	29.41	23.6	1245	–	Excellent light harvesting ability	Huang et al. (2018b)
Rice straw	Hydrothermal treatment	180°C for 24 h	g-MoS_2/ PGBC	50.87	3.96	22.81	266.8	0.126	PGBC with good conductivity; PGBC-OOH; PGBC-OH	Ye et al. (2019)
Cornstalk	Pyrolysis; impregnation	600°C for 6 h; stirred for 4 h; 600°C for 6 h	Biochar/natur-al manganese ore	84.72	10.25	2.79	240.6	0.062	Minerals serve as an electron medium to facilitate the electron transfer and redox	Yang et al. (2021a)

by calcination (Zhang et al. 2017). The composites have a lower S_{BET} (specific surface area) (102.16 $m^2 \cdot g^{-1}$) than that of raw biochar (125.04 $m^2 \cdot g^{-1}$). This phenomenon may be attributed to the reason that semiconductors cover a proportion of the biochar's surface, hence resulting in a decrease in surface area. Moreover, a higher calcination temperature of 500 °C can destroy the structure of biochar, hence resulting in significantly decreased S_{BET} (0.4035 $m^2 \cdot g^{-1}$) of the composite. In contrast, the BET surface area of the Lotus-Leaf-Derived Activated-Carbon-Supported Nano-CdS increased from 734.6 $m^2 \cdot g^{-1}$ to 1245 $m^2 \cdot g^{-1}$ with calcination temperatures that varied from 600 °C to 800 °C (Huang et al. 2018b). It could be assumed that a higher calcination temperature is favorable for woody biomass rather than herbaceous biomass feedstock when preparing catalysts. Consequently, it is critical to reasonably select the feedstock and calcination temperature during the process of catalyst preparation by the calcination method. Moreover, thermal polycondensation is usually used to produce g-C_3N_4 based catalysts, which is actually similar to calcination. For example, biochar@C_3N_4 composites were obtained by a thermal polycondensation process (Pi et al. 2015). Typically, melamine was firstly mixed with biochar and ground for 1 h, the mixture was then heated to 300 °C for 2 h, and the further condensation treatment was performed at 520 °C for 2 h.

3.2 Hydrothermal treatment

Compared with pyrolysis chars, hydrochars possess more OFGs, making it more suitable for being used as an excellent catalyst (Wang et al. 2020d). The hydrothermal treatment process for the synthesis of biochar-based catalysts usually proceeds at the temperature ranging from 90 to 220 °C and a retention time of 2 to 24 h. A ZnO-biochar nanocomposite with high S_{BET} (119.15 $m^2 \cdot g^{-1}$) and V_t (pore volume) (0.16 $m^3 \cdot g^{-1}$) was synthesized by the hydrothermal method at 90 °C for a duration of 2 h (Gholami et al. 2019a). The material with a nano-sized structure can be easily prepared via hydrothermal techniques. The biochar-incorporated Zn-Co-layered double hydroxide (LDH) nanocomposite exhibited good incorporation of Zn-Co-LDH nanostructures into the biochar lattice, and the integration of Zn-Co-LDH nanoflakes with biochar matrix resulted in the formation of a regular-shaped nanocomposite with an improved S_{BET} (95.76 $m^2 \cdot g^{-1}$) compared with the pristine biochar (68.19 $m^2 \cdot g^{-1}$) (Gholami et al. 2020b). Compared with calcination, hydrothermal treatment is more cost-efficient due to milder safety conditions and simple processes without the process of desiccation. The solvothermal method is usually used to prepare TiO_2 or BiOX based catalysts, and it is similar to the hydrothermal method. A biochar@$ZnFe_2O_4$/BiOBr heterojunction was prepared via the simple solvothermal method at 160 °C for 12 h (Chen et al. 2019a). The heterojunction has a lower S_{BET} and V_t of 27.16 $m^2 \cdot g^{-1}$, 0.069 $cm^3 \cdot g^{-1}$ and 30.28 $m^2 \cdot g^{-1}$, 0.056 $cm^3 \cdot g^{-1}$ than pure BiOBr, due to the BiOBr microspheres grown on the surface of biochar causing pore blockage.

3.3 Sol–gel

Sol–gel means that the colloidal suspension or sol is formed from a precursor, such as inorganic metal salts or metal–organic compounds, followed by hydrolysis and polymerization of the precursor (Cui et al. 2021; Silvestri and Goncalves 2019). Tailored properties of the material are advantages of the sol–gel method by controlling the morphology and distribution of the generated inorganic nanomaterials within the polymer matrix. The sol–gel method is mainly used to synthesize biochar-decorated TiO_2 catalysts (Liu et al. 2019c). In TiO_2-decorated biochar-based catalyst, the TiO_2 nanoparticles are agglomerated on the surface of biochar, and the crystal phase structure, average size, and dispersion of TiO_2 upon the biochar greatly depend on the sol–gel decomposition temperature (Mian and Liu 2018). After the solution reaction step, it is easy to uniformly and quantitatively incorporate some elements to improve catalyst performance. It is generally believed that the diffusion of the components in the sol–gel system is in the nanometer range, and the reaction is easier to proceed and the temperature is low compared with the solid phase calcination reaction. For example, Xie (Xie et al. 2019) used absolute ethanol and acetic acid as the solvent to prepare Zn doping TiO_2/BC catalyst with S_{BET} of 169.1579 $m^2 \cdot g^{-1}$ by simple sol–gel method at room temperature. The result indicated that the doping of zinc elements via the sol–gel method may make TiO_2 easier to load on biochar, and effectively reduce the agglomeration of TiO_2 and crystal size. However, sol–gel is just a critical step to prepare catalysts, and it needs to conduct a further calcination after the process of depositing catalytic nanoparticles on the biochar surface (Zhang et al. 2017). Moreover, there are some shortcomings involved with the sol–gel method. For example, the cost of raw metal alkoxide is relatively high, and organic solvents might be toxic, the entire sol–gel process usually takes a long time, and gas and organic matter will escape and shrinkage during the drying process.

3.4 Impregnation

3.4.1 Metal (oxides)

In this method, active metallic species are incorporated into biochar structures by mixing feedstock with metal

precursors, forming active interfaces and binding sites (Tam et al. 2020). This method could have a great enhancement for biochar-based catalysts on the adsorption capacity, catalytic performance and magnetism (Pan et al. 2021). The magnetic nitrogen doped biochar catalysts were prepared through impregnating biochar with mixtures of $Co(NO_3)_2$ and $FeSO_4$ under an oxygen-limited condition, followed by calcination at a desired temperature (400–800 °C) for 4 h (Liu et al. 2019a). The composite calcined at a higher temperature had higher SBET (150.7 $m^2 \cdot g^{-1}$) and V_t (0.081 $cm^3 \cdot g^{-1}$) than that calcined at comparatively low temperatures, which is not consistent with the previous study (Zhang et al. 2017), despite this identical biomass feedstock. This phenomenon can be attributed to the formation of a large number of $CoFe_2O_4$ crystals on the surface of biochar by impregnation, which could contribute to the stability of the biochar pore structure. Moreover, a higher calcination temperature can obtain a high graphitization degree structure, which is conductive to the charge transfer process and helpful for promoting electron transfer (Wang et al. 2018a). A TiO_2/Fe/Fe_3C-biochar composite was synthesized by impregnating sewage sludge and different ratios of nanoparticles with chitosan, subsequently thermal decomposition at 800 °C (Mian and Liu 2019). NPs (nanoparticles) ratio and chitosan support have significant influence on the properties and catalytic activity of catalysts,and high content of Fe impregnation reduces surface area and active site due to Fe^0 agglomeration. Nevertheless, impregnation often produces composites rather than carbonaceous biochar, demanding scrutiny comparison among bare biochar, impregnated composites, and the exhausted catalysts (Tam et al. 2020). The precipitation method can be classified as one of the impregnation methods, and the difference is that precipitates are formed and deposited on the biochar surface when caring out the impregnation process. The biochar@$CoFe_2O_4$/Ag_3PO_4 was synthesized by a facile in-situ precipitation process via using ethylene glycol as the solvent, followed by impregnating biochar@$CoFe_2O_4$ with mixtures of $AgNO_3$ and Na_2HPO_4 (Zhai et al. 2020). Similarly, the composite exhibited a lower S_{BET} (21.85 $m^2 \cdot g^{-1}$) and V_t (0.059 $cm^3 \cdot g^{-1}$) than raw magnetic biochar, the introduction of magnetic biochar had little effect on the crystal structure of Ag_3PO_4 by impregnation process, and the intensity of crystal characteristic peaks of the photocatalysts varies with the change of loading ratio.

3.4.2 Non-metallic

Attention has been increasingly paid to incorporating non metallic elements (such as N, S, P, B) into biochar-based catalysts for the catalytic activity recently (Wan et al. 2022). Due to the different atomic radiuses, atomic orbitals and electronegativity of these elements, this method could promote the electron density, reactive-active moieties, defective sites and reusability by chemically modifying and modulating the inherent carbon configuration (Tam et al. 2020; Wan et al. 2020; Yu et al. 2020), and it shows the superiority over many other methods. N-doped biochar-based catalysts could form pyridinic-N, pyrrolic-N, quaternary-N, and pyridone-N-oxide through the polymerization reaction with oxygen- containing functional groups on the surface of biochars, which increase the surface sorption sites, basicity and positive charges (Chen et al. 2018; Huang et al. 2022; Kasera et al. 2022). It was reported that the CO_2 uptake of the N-doped hickory biochar was 31.6%-55.2% higher than that of the corresponding pristine and ball-milled biochars. Chen found that N-doped biochars show a synergetic effect on the formation of phenols by combining the advantages of activated carbon, active functional groups, and NH_3, and it also inhibits the generation of O-species and acetic acid while promotes the formation of aromatics (Chen et al. 2020). Biochar-based catalysts doping S could improve the persulfate activation capacity of sludge biochar-based catalysts via enhancing the electron shuttling capacity in nonradical pathways (Yun et al. 2018). Wang prepared sewage sludge biochars incorporating zigzag-edge sulfur (SSB), and it effectively activated the sp^2-hybridized graphene lattice, which generated more Lewis acid and basic sites. 93.6% of bisphenol A (BPA) removal was achieved by SSB/PMS within 60 min (Wang et al. 2020b). The doping of P could introduce functionality onto biochars to realize chemical activation based on the low electronegativity and the large atomic radius of P (Suo et al. 2019; Zhou et al. 2022a). Zhou prepared the P-doped biochar composites with high specific surface area, mesoporous ratio and abundant P-containing functional groups, and P-O-$C_{aromatic}$ and $C_{aromatic}$-PO3/$C2_{aromatic}$-PO2 groups are the active sites for chemical adsorption of methylene blue (Zhou et al. 2022b). B dopants could modulate the electron distribution and physicochemical properties of sp^2-hybridized carbons, and it was found that the biochar materials introduced B, which acts as the Lewis acid site, enhanced the surface affinity towards peroxydisulfate (PDS) and modulated the electronic structure of catalysts, and evidently resulted in superior electron transfer rate long-term durability and catalytic capacity owing to the high stability boron sites (Liu et al. 2020b; Sun et al. 2018).

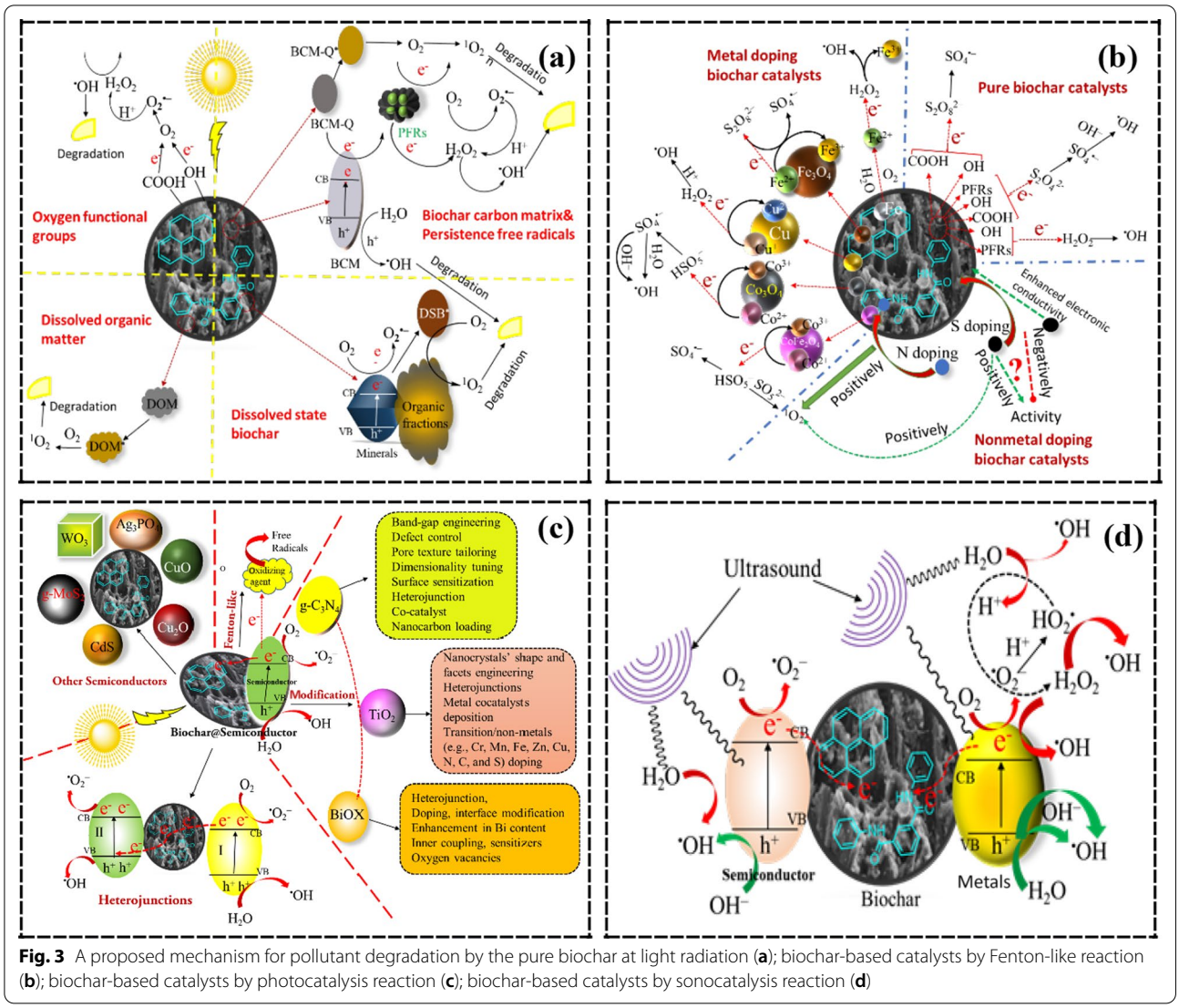

Fig. 3 A proposed mechanism for pollutant degradation by the pure biochar at light radiation (**a**); biochar-based catalysts by Fenton-like reaction (**b**); biochar-based catalysts by photocatalysis reaction (**c**); biochar-based catalysts by sonocatalysis reaction (**d**)

4 Biochar-based catalyst applications in pollution control

Biochar-based catalysts have been widely used for the removal of contaminants in water and soil. Moreover, biochar-based catalysts have been widely used in different systems, including redox systems, Fenton-like systems, sonocatalytic systems and photocatalytic systems (Fig. 3) (Table 3).

4.1 Biochar composite for redox systems

Organic contaminants can be directly degraded by biochar without the addition of oxidants (Lyu et al. 2020). PFRs in biochar can transfer electrons to O_2 to produce the superoxide radical anion and hydrogen peroxide, which react further with PFRs to produce $^{\cdot}OH$ (Fang et al. 2015). Biochar carbonization temperature is a critical factor affecting the generation of PFRs, which further affects the degradation of organic pollutants. In a previous study, the rice husk-derived biochars exhibited the degradation rate for 1,3-dichloropropene initially decreased from 0.00152 h^{-1} to 0.00073 h^{-1} and subsequently increased to 0.00305 h^{-1} with an increasing pyrolysis temperature range from 300 to 700 °C (Qin et al. 2017). A certain high temperature promotes the formation of PFRs, but excessively high temperatures may cause the cracking and reorganization of the organic structure, resulting in the elimination of PFRs (Fang et al. 2015). Besides, DOM with abundant PFRs derived from a sugar beet tailing and Brazilian pepper biochars, serving as both electron donor and electron acceptor, exhibited 100% reduction of Cr(VI) (Dong et al. 2014). Moreover, the introduction of metal could significantly improve

Table 3 Applications of various biochar-based catalysts in pollutant control

	Catalysts	Reaction conditions	Removal performance	Influence factors	Driving mechanisms	References
Redox system	Fe@biochar	[*As(III)/Cr(VI)*] = 0.03 M; [catalyst] = 1 g·L^{-1}; t = 48 h; T = 323 K; pH = 6.5	91.3% for As(III); 85.9% for Cr(VI)	Temperature; O-functionality; amorphous ferrous mineral; minerals (e.g., Ca, Mg, K)	Fe@biochar generated more reactive ·OH by reducing the O_2 and enhanced the redox-related transformation of As(III)/Cr(VI)	Xu et al. (2022)
	Cotton straw biochar	$[E2]_0 = [EE2]_0$ = 10 μM; [NH_2Cl] ~0.15 mM, 24 h; $[Cot350]_0$ = 1 g·L^{-1}; $[NH_4Cl]_0$ = 0.30 mM; $[FAC]_0$ = 0.15 mM; T = 25°C; $[phosphate\ buffer]_0$ = 5 mM; pH = 9	95% of E2 and EE2; 87% of E2 and 75% of EE2 within 24 h	Cl^- inhibits but NH_4^+ and HCO_3^- promote removal	Nitrogen and silicon elements of biochar activated NH_2Cl to generate ·NO for the degradation of the EDCs	Wang et al. (2019c)
	Co_3O_4@ biochar	[catalyst] = 4.0 mg; [$NaBH_4$] = 1 mL 250 mM; [*p*-nitrophenol] = 1 mL 0.68 mM	100% after 10 cycles	Pyrolysis atmosphere; temperature	The catalytic performance of biochar is contingent on both pore structure and Co_9S_8	(Kwon et al. 2018)
	Ag@biochar	[*Cr (VI)*] = 0.02 M; T = 323 K; t = 20 min; [Ag@biochar] = 1 g·L^{-1} and HCOOH (95% v/v; 3.97 mL)	100% within 20 min; 93% after 2 cycles	Particle size of Ag; dependent on temperature; minerals (e.g., Ca, Mg, K)	Follows a CO reduction mechanism	Liu et al. (2016)
	Pine needles biochar	[*diethyl phthalate*] = 5 mg·L^{-1}; [oxygen] = 0.2 mL·min^{-1}; [P300] = 1 g·L^{-1}; $[ethanol]_0$ = 10 mM; T = 25°C; pH = 7.4	100%	High oxygen concentration enhances removal	FRs in biochar transfer electrons to O_2 to form $O_2^{\cdot-}$ and H_2O_2, which reacts with FRs to produce ·OH	Fang et al. (2015)
Fenton-like system	Biochar/natural manganese ore	[BPA] = 20 mg·L^{-1}; [PMS] = 1.0 mM; [catalyst] = 1.0 g·L^{-1}; pH = 6.5; t = 2 h	95.9% within 2 h	Catalysts dosage; HCO_3^-	PMS activated via a nonradical mechanism to metastable state, BPA transferred electrons to the metastable PMS through the catalyst	Yang et al. (2021a)
	Sch@biochar	[*SMX*] = 10 mg·L^{-1}; [H_2O_2] = 2.0 mM; [catalyst] = 1.0 g·L^{-1}; pH = 3.0; t = 60 min; ultrasonic power = 300 W	100%	Catalysts dosage; pollutant concentration; pH	Hydroxylation; the oxidation of the amino groups; the cleavage of the S–N bonds	Yang et al. (2021b)
	Oxidation biochar-Fe_3O_4	[*tetracycline*] = 20 mg·L^{-1}; [PS] = 10 mM; [catalyst] = 0.4 g·L^{-1}; pH = 3.0; t = 2 h	92.3% within 2 h	pH; $H_2PO_4^-$	Involving generation of $SO_4^{\cdot-}$, ·OH and $^1O_2$	Pi et al. (2019)
	N-biochar @$CoFe_2O_4$	[*MET*] = 10 mg·L^{-1}; t = 360 min [catalyst] = 200 mg·L^{-1}; [PMS] = 0.5 mM; pH = 3–11	3cycles, > 80%	Temperature; pH-dependent and favorable at neutral and weak basic conditions	$SO_4^{\cdot-}$, ·OH and $^1O_2$ participated into degradation	(Liu et al. 2019a)

Table 3 (continued)

	Catalysts	Reaction conditions	Removal performance	Influence factors	Driving mechanisms	References
Sonocatalytic system	Ti-BC hydrogel beads	[*CIP*] = 30 mg·L^{-1}; [catalyst] = 1 g·L^{-1} t = 120 min; ultrasonic power = 300 W	62% after four cycles	Na_3PO_4 inhibits removal; pH; minerals; ultrasonic power; catalyst amount; temperature	Cavitation, nucleation, growth, and implosion of microbubbles	Afzal et al. (2022)
	(Fe-Cu-LDH) /biochar	[*cefazolin sodium*] = 0.1 mM; [catalyst] = 1 g·L^{-1}; ultrasonic power = 300 W; t = 80 min; pH = 6.5	97.6% during 80 min; 9% drop after five cycles	Ultrasonic power; pH; dissolved gases; oxidants; organic/inorganic scavengers	h^+ reacts with H_2O, OH^- to generate ·OH, e^- reacts with O_2 to form $O_2^{-\cdot}$, which reacts with h^+ to generate ·OOH	(Gholami et al. 2020a)
	ZnO-biochar	[*GMF*]$_0$ = 20 mg·L^{-1}; [catalyst] = 1.5 g·L^{-1}; pH = 5.5; ultrasonic power = 300 W	83.7% COD removal within 90 min; 10% loss of degradation after five runs	Pollutant concentration; solution turbulence; catalysts dosage; ultrasonic irradiation powers; gas addition	h^+ reacts with OH^- and H_2O to generate ·OH, hot spots product ·OH	Gholami et al. (2019a)
	CeO_2-H@biochar	[*RR84*] = 10 mg·L^{-1}; [catalyst] = 1 g·L^{-1}; t = 360 min; pH = 6.5; ultrasonic power = 300 W	98.5% within 60 min; 87.1% after five cycles	Initial RR84 concentration; pH; catalyst amount; ultrasonic power	Sonication generates OH and H radicals, and enhances redox/ electronic properties and peculiar ceria-BC synergistic effect	Khataee et al. (2018)
Photocatalytic system	Biochar@$CoFe_2O_4$/Ag_3PO_4	[*BPA*] = 20 mg·L^{-1}; visible-light irradiation; [catalyst] = 0.5 g·L^{-1}; t = 60 min	80.23% mineral-ization in 60 min; 58.96% after 4 cycles	Mass ratio of magnetic biochar in catalysts	Z-scheme photocatalytic mechanism, h^+ and $\cdot O_2^-$ are active species	Zhai et al. (2020)
	Fe_3O_4 based glucose magnetic hydrochar	VL irradiation; [*Cell*] = 8.0 log cfu·mL^{-1}; [MHC] = 200 mg·L^{-1}; [PS] = 2 mM; T = 25°C; pH = 3 ~ 9	Completely treat 8.0 log *E. coli* cells, 40 min	pH; dissolved O_2	PS activation by ≡Fe(II) of Fe_3O_4 and photo-generated electron captured by PS were major processes	Wang et al. (2020d)
	Cu_2O-CuO@biochar	[*RO29*] = 20 mg·L^{-1}; [catalyst] = 1 g·L^{-1}; pH = 8.7; UV light irradiation	94.12% in 90 min; 79.62% COD removal in 180 min	BC content; scavengers; enhancers; dosage of catalysts and pollutants	h^+, $O_2^{\cdot-}$ and ·OH are major reactive agents	Khataee et al. (2019)
	Biochar carbon-doped TiO_2/CuO	[*ammonia*] = 100 mg·L^{-1}; 25°C for 24 h; sunlight and UV light irradiation	99.7% under UV light while 60.7% under sunlight	Calcine temperature; pH; photocatalyst dosage	h^+, $\cdot O_2^-$ and ·OH are main active species	Peng et al. (2019)
	Zn-Co-LDH@biochar	[catalyst] = 0.75 g·L^{-1}; [*GMF*]$_0$ = 15 mg·L^{-1}; pH = 2.5; UV light irradiation	92.7% in 130 min; < 10% drop after five runs; 80% COD removal in 200 min	Solute concentration; photocatalyst dosage	·OH is major reactive agents	Gholami et al. (2020b)
	TiO_2/biochar	[*MO*] = 20 mg·L^{-1}; [catalyst] = 0.25 g·L^{-1}; UV irradiation time; 150 min	83.23% mineral-ization, 76.56% after 5 runs	Weight ratio of biochar to Ti	h^+, $\cdot O_2^-$, ·OH as active species	Lu et al. (2019)
	TiO_2/BC	pH = 8.71; [KN-R] = 30 mg·L^{-1}; [catalyst] = 6.0 g·L^{-1}; UV high pressure xenon lamp	99.71% within 60min when PH=1; 73.98 ± 0.13% until fifth cycle	Illuminant; pH; catalysts dosage; KN-R concentration;	h^+, $\cdot O_2^-$, ·OH as active species	Zhang and Lu (2018)

Table 3 (continued)

	Catalysts	Reaction conditions	Removal performance	Influence factors	Driving mechanisms	References
	Activated carbon-TiO_2 Olive pits-TiO_2 Wood shaving-TiO_2	Visible lights; pH = 3; [*CrVI*] = 10 ppm; [catalyst] = 0.5 g·L^{-1}; [Tartaric acid] = 10 mg·L^{-1}	Completely reduced after 30 min, 50 min and 130 min	Surface area and porosity of catalysts; composite	Photoreduction by e-, sensitized mechanism, carboxyl-TiO_2 surface-complex mediated, charge transfer	Djellabi et al. (2019b)
	TiO_2/pBC	[*SMX*] = 10 mg·L^{-1}; pH = 4; [photocatalyst] = 1.25 g·L^{-1}	91.27% in 3 h; 57.44% of COD	Calcination condition; inorganic anions; pH	$^{\cdot}O_2^-$, $^{\cdot}OH$ are major reactive agents	Zhang et al. (2017)
	Ti-coupled N biochar	[*RhB*] = 20 mg·L^{-1}; [catalyst] = 1 g·L^{-1}; 20°C; visible-light irritation	52.53% TOC removal	Amount of Ti precursor	–	Li et al. (2018)
	Zn-TiO_2/biochar	[catalyst] = 1.25 g·L^{-1}; [*SMX*] = 10 mg·L^{-1}; T = 25°C; pH = 5.03; visible light irritation	81.21% in 3 h	Zn content; solution pH; catalyst dosage; anions	$^{\cdot}O_2^-$, $^{\cdot}OH$ as reactive oxygen species	Xie et al. (2019)
	TiO_2-lignocellulosic biomass@Fe_3O_4	visible light; [*dyes and Cr(VI)*] = 10 ppm; [photocatalyst] = 0.25 g·L^{-1}	100, 75 and 81% in 1 h for MB, RhB and CR; 100% within 40 min for Cr(VI)	Pollutant; catalyst; Tert-butyl alcohol concentration; pH; metallic cations	Dyes are oxidized by $^{\cdot}OH$, Cr(VI) is reduced	Djellabi et al. (2019a)
	TiO_2/Fe/Fe_3C-biochar	pH = Not adjusted (6.7); [catalyst] = 1 g·L^{-1}; [H_2O_2] = 0.57 M; [*MB*] = 200 mg·L^{-1}	376.9 mg·L^{-1} in 300 min	Ratio of sludge; chitosan; $Ti(OBu)_4$; glutaraldehyde; $FeCl_3$; H_2O_2; pH	$^{\cdot}OH$ and some $O_2^{\cdot-}$perform in degradation and mineralization	Mian and Liu (2019)
	g-C_3N_4 modified biochar	[*MB*] = 5.4 mg·L^{-1}; [*MO*] = 16 mg·L^{-1}; [*p-nitrophenol*] = 32 mg·L^{-1}; [catalyst] = 0.45 g·L^{-1}; 18 W LED light	91% decoloriza-tion	Biochar/melamine mass ratios; pH	h^+ and $O_2^{\cdot-}$ are the primary oxidative species	Pi et al. (2015)
	Biochar@g-C_3N_4 core–shell photocatalysts	[catalyst] = 0.5 g·L^{-1}; [*TC*] = 10 mg·L^{-1}; light irradiation	~55%, no evident activity loss after 4 cycles	Amounts of g-C_3N_4	h^+ and $^{\cdot}O_2^-$ play main roles as the active species	Wang et al. (2018b)
	Fe_3O_4/C/g-C_3N_4	Visible light; pH = 2; [catalyst] = 0.2 g·L^{-1}; [Cr(VI)] = 20 mg·L^{-1}	100%, 20.9-fold that over g-C_3N_4 for Cr(VI)	pH	Reduced mainly by the e^- directly, subordinately reduced by $^{\cdot}O_2^-$	Ding et al. (2018)
	Magnetic biochar supported g-C_3N_4/$FeVO_4$	pH = 5.5; T = 30°C; [catalyst] = 0.5 g·L^{-1}; [methyl paraben and 2-cholrophenol] = 20 mg·L^{-1}	98.4% of MeP and 90.7% of 2-CP in 60 min	Solar; ozone; pH; scavengers	h^+, $^{\cdot}O_2^-$, $^{\cdot}OH$ as active species	Kumar et al. (2017)

Table 3 (continued)

	Catalysts	Reaction conditions	Removal performance	Influence factors	Driving mechanisms	References
	Biochar@$Bi_2O_2CO_3$/g-C_3N_4/$CoFe_2O_4$	[catalyst] = 0.5 mg·mL^{-1}; [*PQT*] = 20 ppm; pH = 7.2; T = 30 ± 0.5°C	99.3% under visible light in 90 min	pH, H_2O_2, anions, ozone and PMS	$SO_4^{\cdot-}$ and $^{\cdot}OH$ are main active species	Kumar et al. (2018)
		[*4-NP*] = 10 mM; N_2; [$NaBH_4$] = 0.05 M; BCBF: 4-NP: $NaBH_4$ = 1: 10:700;	Complete conversion in < 5 min			
		[catalyst] = 100 g·L^{-1}; t = 1 h; [CO_2] = 0.5 ml; Xe arc lamp 880 W	CH_4 (~ 119 μmol g^{-1}), CO (~ 131 μmol g^{-1}) and O_2 (~ 242 μmol g^{-1})		h^+ reacts with H_2O to generate H^+ and O_2, H^+ reacts with CO_2 and e^- to generate CH_4	
	Biochar/BiOX (X = Br, Cl)	[catalyst] = 1 g·L^{-1}; [*MO*] = 0.6 M; t = 2.5 h; visible light irritation	82% for 2.5 h	Ratio of C/BiOX	h^+, $^{\cdot}OH$ and $^{\cdot}O_2^-$ function as active species	Li et al. (2016)
	CdSe/HTC composites	[*TC*] = 20 mg·L^{-1}; T = 25 ± 1°C; [catalyst] = 0.5 g·L^{-1}; t = 80 min; visible light irradiation	35.86% mineralization	Water substrates; pH; salt; TC concentration; catalyst dosage; co-existing ions	e^- produces $^{\cdot}O_2^-$, which reacts with h^+ to generate $^1O_2$; $^{\cdot}O_2^-$, h^+, $^1O_2$ are main active species	Men et al. (2019)
	CdS@LAC-800	[organic dyes] = 40 mg·L^{-1}; [catalyst] = 100 mg·L^{-1}; visible light	97.8% in 60 min for MO; 96.3% at 150 min for MB	Activated carbon; production temperatures	Efficient light harvesting; h^+, $O_2^{\cdot-}$, $^{\cdot}OH$ and H_2O_2 are main active species	Huang et al. (2018b)
	g-MoS_2/PGBC	[*TC*] = 20 mg·L^{-1} 50 mL; visible light irradiation	> 40% TOC removal after 60 min	Graphitization degree and conductivity of biochar; pH; coexisting anions	h^+ and $^{\cdot}OH$ are predominant active species	Ye et al. (2019)

the oxidation–reduction activity of pure biochars. For instance, biochar-coated Fe(0) composite exhibited more than 90% removal of 2,4,6-Trinitrotoluene in 5 h, and the biochar of the composite may act as an electron transfer mediator (Oh et al. 2017). An Ag nanoparticle-embedded biochar hybrid material can completely catalytically reduce Cr(VI) using formic acid as a reducing agent, and the particle size of Ag plays an important role in this process (Liu et al. 2016). Obviously, pure biochar or biochar-coated metal composites can efficiently achieve an almost complete reduction of Cr(VI). The properties of pure biochar need to be adjusted to enhance its catalysis-reaction. The cost and risks of heavy metal release of the biochar-coated metal composite may be high, due to the introduction of metal. Biochar catalyst selection for the pollutant oxidation and reduction should be based on the biochar characteristics, cost, and environmental risks.

4.2 Biochar-based catalysts for Fenton-like systems

4.2.1 Pure biochar

The biochars can effectively catalyze H_2O_2 to form ROS, resulting in the degradation of pollutants. The pyrolysis temperature of biochar influenced •OH generation in the presence of H_2O_2. It was reported that wheat-derived biochars at higher temperatures led to a higher yield of •OH during H_2O_2 activation, and the degradation efficiency of sulfamethazine (13.7 μM) went up from 93.4% to 100% with the increase of pyrolysis temperature, and the drawback is that reactivity was inhibited by the adsorption of sulfamethazine on their surface (Huang et al. 2016).

The peroxide could be effectively catalyzed by OFGs and PFRs of biochars to form ROS or sulfate radicals for pollutant degradation (Xia et al. 2020). The sewage sludge biochar was proven to be an efficient persulfate activator for pollutant degradation, a high mineralization efficiency of ~ 80% for BPA could be achieved by PMS at a biochar dosage of 0.2 $g{\cdot}L^{-1}$ within 30 min, and $^1O_2$ was the main reactive species (Huang et al. 2018a). The pyrolysis temperature significantly affects the activity of the activation reaction. In a study, N-doped graphitic biochars (N-BCs) were used as catalysts for PDS activation. In particular, N-BC derived at 900 °C (N-BC900) exhibited the highest degradation rate, and it could completely degrade phenol, sulfamethoxazole (SMX) and BPA in 20 min, and Orange G in 60 min at 20 ppm, which was 39-fold of that on N-BC400 (Zhu et al. 2018). Different from the radical-based oxidation in N-BC400/PDS via the PFRs, $^1O_2$ and nonradical pathways dominate the process. Besides, the contributions made by organic matter, acid-soluble substance (ASS), carbon matrix (CM), and basal part (BSP) in a magnetic nitrogen-doped sludge-derived biochar (MS) for activation reaction were significantly different, and it was reported that ASS was the most important contributor for MS-400/600 while CM took the absolute dominance for MS-800, ASS and CM took the responsibility for the generation of $SO_4^{\cdot-}$ and $^{\cdot}OH$ in MS-800/PDS system (Yu et al. 2019).

4.2.2 Transition metals-based biochar catalysts

Transition metals, such as iron, copper, cobalt and so on, can efficiently activate oxidants to generate ROS. Due to the excellent performance and low toxicity, iron-based catalysts have attracted extensive attention. Nanoscale zero valent iron (nZVI) and magnetite (Fe_3O_4), as two common potential alternative sources of Fe^{2+}, can be used to activate oxidants for pollutant degradation. More than 70% of ciprofloxacin was removed, using BC/nZVI activating H_2O_2 (20 mM) in acidic conditions, and $^{\cdot}OH$ oxidation was the primary pathway in the process (Mao et al. 2019). Similarly, the pyrolysis temperature significantly affects the catalytic properties of magnetic biochar by affecting the size distribution of iron oxides, especially Fe (II) content in these composites. In a study, metronidazole was rapidly and completely degraded by the magnetic biochar at the temperature of 400 °C (SMBC400) activating H_2O_2, and the rate of which was higher than that of SMBC300 and SMBC500 (Yi et al. 2020). Recently, a $^{\cdot}SO_4^-$ mediated photocatalysis associated with a Fenton-like system was used for bacterial inactivation. In this study, Fe_3O_4-based magnetic hydrochar (MHC) was used for persulfate (PS) activation under visible light. Complete treatment of 8.0 log *E. coli* cells was reached within 40 min in visible light /PS/MHC system, suggesting higher removal than that of PS/MHC system (Wang et al. 2020d). As a result, photo-Fenton-like systems may be a promising water disinfection technology. The Cu and Co-based biochar catalysts were also used to activate peroxide or hydrogen peroxide for organic pollutant degradation. A solid digestate-biochar-Cu NP composite (0.5 $g{\cdot}L^{-1}$) exhibited a tetracycline (TC) (200 $mg{\cdot}L^{-1}$) degradation of 97.8% in the presence of H_2O_2 within 6 h of reaction time, which was mainly attributed to Cu(II)/Cu(I) redox reaction and the electron-transfer process of FRs in biochars (Fu et al. 2017). The degradation capacity for TC is well above that of almost all other photocatalysts. It was reported that nearly complete removal of chloramphenicol (30 $mg{\cdot}L^{-1}$) was achieved in a Co_3O_4-BC/PMS system within 10 min, the outstanding performance of which mainly stems from the synergistic effect of the conducting BC and the Co^{3+}/Co^{2+} redox reaction (Xu et al. 2020). In addition, non-metal, such as S and N doping can further promote the activity performance of Co-based biochar catalysts. It was reported that the dinotefuran decomposition of S-doped Co_3O_4 composite increased by 1.71 times as compared to the S-free sample, which was attributed to the enhanced generation

of $^1O_2$ and various radicals by S incorporation (Du et al. 2020). Similarly, a higher pyrolysis temperature of biochar could improve PDS activation reaction. A N-doped graphitic biochar (SDBC-900) showed a faster degradation with complete SMX removal compared with 33.0% and 84.9% on the biochar pyrolyzed at 400 and 700 °C in 45 min (Ho et al. 2019). During this process, the SDBC 900-acid played versatile roles in PDS activation. While S doping is not always positive for PMS activation, according to a previous study, a heteroatom (N and S) doping biochar was used for the catalytic degradation of metolachlor through activating PMS, N-doping positively whilst S-doping negatively influenced the degradation process (Ding et al. 2020). In conclusion, the biochar-based catalysts exhibited better degradation performance in the Fenton-like system than that of photocatalysis system for refractory emerging organic pollutants, such as TC, SMX, ciprofloxacin and so on. However, pollutants degraded by biochar-based catalysts in the Fenton-like system might generate high-cost and ecotoxicity risks, due to the induction of peroxide (Li et al. 2022). Based on the cost-effectiveness, photo-Fenton-like systems may be a promising development direction in degradation-resistant wastewater treatment.

4.3 Biochar-based catalysts for sonocatalytic systems

The application of ultrasound as a primary source to stimulate chemical reactions has received increasing attention. However, there are some disadvantages, including long treatment time and huge consumption of energy, biochar-based materials can act as suitable sonocatalysts to counter these deficiencies (Wang et al. 2019a). As the name implies, the ultrasonic frequency had a substantial effect on the sonocatalytic reaction (Gholami et al. 2019b). Recently, a series of biochar-based composite catalysts, including pure biochar, transition metals, lanthanide metal and semiconductor-based biochar composites were synthesized.

Biochar, as a sonocatalyst, is more useful in low-frequency ultrasound systems for organic pollutant degradation. In a previous study, a peat-moss derived biochar exhibited higher removal efficiency for rhodamine B (100 $mg{\cdot}L^{-1}$) at 40 kHz (51.8%) than that at 300 kHz (26.2%) after 1 h, due to less dispersion of the biochar in the solution at 300 kHz, and stronger sonophysical effects at 40 kHz, which significantly enhanced the sonochemical oxidation reactions on the surface of the biochar (Kim et al. 2018). Similarly, Fe, Cu, Mn and Zn, as common transition metals, are usually used to prepare catalysts owing to the characters of high efficiency, non-toxicity, low cost and environmental friendliness. For instance, Fe-Cu layered double hydroxide/biochar exhibited a high sonocatalytic efficiency of 97.6% for cefazolin sodium (0.1 mM) at an ultrasonic power of 300 W within 80 min (Gholami et al. 2020a). In a study, two types of hierarchically structured manganese dioxide/biochar nanocomposites (MnO_2/BCs) were prepared for BPA degradation in an ultrasound-assisted heterogeneous Fenton-like system. In this process, the crystalline properties of the nanocomposites affected their catalytic activity, and the α-MnO_2/biochar exhibited complete removal of BPA (100 μM) in the presence of H_2O_2 (10 mM) by using an ultrasonic power of 130 W within 20 min (Jung et al. 2019). Cerium oxide (CeO_2) and ZrO_2, as oxides of the lanthanide metal, have been widely used to couple with biochars as heterogeneous catalysts. The prepared CeO_2-H@BC nanocomposites exhibited the best Reactive Red 84 degradation efficiency, which was enhanced with the increase in ultrasonic power. In this process, a 98.5% degradation was obtained with an ultrasonic power of 450 W and an initial Reactive Red 84 concentration of 10 $mg{\cdot}L^{-1}$ (Khataee et al. 2018). A ZrO_2-biochar exhibited 96.8% degradation efficiency with an initial Reactive Yellow 39 concentration of 20 $mg{\cdot}L^{-1}$ and ultrasonic power of 300 W (Khataee et al. 2017b). The high sonocatalytic activity could be explained by sonoluminescence and hot spot mechanisms. Interestingly, the TiO_2-biochar nanocomposites could be used as sonocatalyst for dye degradation, the mechanisms of which are similar to those of ZrO_2-biochar, and degradation efficiency of 97.5% was observed at initial Reactive Blue 69 concentration of 20 $mg{\cdot}L^{-1}$ and ultrasonic power of 300 W after 80 min (Khataee et al. 2017a). In conclusion, biochar-based composite catalysts could efficiently degrade (almost 100%) cationic dyes, and the performance increased with the increase of ultrasonic power, whereas the tendency was opposite to pure biochar. To develop new biochar-based composite and ultrasound-assisted heterogeneous Fenton-like system for the removal of emerging persistent organic pollutants may be currently an important development direction.

4.4 Biochar-based catalysts for photocatalytic systems

4.4.1 Pure biochar

Pure biochar can directly generate ROS without oxidants for organic pollutant degradation under UV light irradiation. It was reported that 100%, 95% and 89% of 5.0 $mg{\cdot}L^{-1}$ diethyl phthalate were degraded in pine needles, wheat and maize straw biochar (pyrolysis at 300 °C) suspensions in the presence of O_2, respectively, with the reaction time of 24 h (Fang et al. 2015). In this process, Free radicals (FRs) in biochar transferred electrons to O_2 to produce the $^{\cdot}O_2^-$ and H_2O_2, which reacted further with FRs to produce $^{\cdot}OH$. Biochar carbon matrix (BCM) and DOM can induce the generation of ROS under solar irradiation. In a previous study, the photogeneration of

ROS from biochar suspension was investigated, and the results indicated that BCM accounted for 63.6–74.6% of $^{\cdot}OH$ and 10–44.7% of $^1O_2$ formation, while DOM derived from biochar generated 46.7–86.3% of $^1O_2$ and 3.7–12.5% of $^{\bullet}OH$, and almost 59–72% diethyl phthalate degradations were achieved within 120 min under UV light by pine needle and wheat straw biochars (Fang et al. 2017). Moreover, it was reported that DOM strongly influences the photodegradation of organic pollutants, which varies depending on the structure of DOM. After exposure to UV light, the aromaticity and molecular weight of the DOM declined due to photo transformation, and significant enhancement was observed in imidacloprid photodegradation (almost 90% in 90 min) in the presence of biochar-derived DOM (Zhang et al. 2020a). It is noted that the biochars exhibited different performance, due to differences in biochar pyrolysis temperature. Besides, the pyrolysis temperature affects the photocatalytic activity of dissolved state biochar (DSB). It was found that the photocatalytic efficiency of DSB increased with the decrease of pyrolysis temperature, and DSB300 had the greatest gradation of 60% for atorvastatin (10 μM) in 5 h under sunlight. The greatest performance could be attributed to the dual role of DSB, the mineral and organic carbon components of which can act as heterogeneous photocatalysts and photosensitizers to synergistically enhance electron–hole separation, and contribute to the formation of $^1O_2$ and triplet-excited state (3DSB*) (Shi et al. 2020). Consequently, FRs, BCM, DOM, and DSB play a critical part in enabling biochars to participate in photocatalytic reactions. To manufacture biochars with targeted photocatalytic performance, it is essential to define the correlation of photochemical reactivity with the structure and moieties of biochars.

4.4.2 Titanium dioxide

Titanium dioxide, as the most commonly used photocatalyst, provides a set of beneficial redox properties (Hu et al. 2020). However, the photocatalytic activity is hampered by limited light absorption and the high recombination of charge carriers (Naldoni et al. 2019). To mitigate this limit, different approaches have been explored for the material's assembly, such as nanocrystals' shape and facet engineering, heterojunction construction, and metal co-catalyst deposition (Chen et al. 2010). The previous researches had indicated that biochars can serve as a support for TiO_2 to remedy the above shortcomings. The TiO_2/biochar composite exhibited a higher decolorization efficiency of 96.88% than that of single TiO_2 for methyl orange (Lu et al. 2019). An obvious enhancement of absorption in the visible light band was obtained owing to the presence of biochar, which can transfer electrons or serve as acceptor, and the absorbance in the visible light band with the increase of the ratio of biochar to TiO_2. In addition, early work on doped TiO_2 employed transition metals (e.g., Cr, Mn, Fe, Zn and Cu) introduced as substitutional atoms inside the crystalline habit to generate 3d electronic states lying in the range 0.5–1.5 eV below the conduction band (CB) of TiO_2, thus providing visible light absorption, for example, the TiO_2/Fe/Fe_3C-biochar obtained a rising adsorption in the visible-light region due to the charge transfer of Ti^{3+}, Si, Al, and Fe, and the methylene blue removal capacity evaluated as 376.9 $mg{\cdot}L^{-1}$ (Mian and Liu 2019). However, metal doping may show an unfavorable trade-off between absorption and photocatalytic activity, resulting in increased charge recombination via newly formed deep electronic levels (Naldoni et al. 2019). For instance, Zn-TiO_2/biochar exhibited a lower degradation (81.21%) (Xie et al. 2019) than that of TiO_2/biochar (91.27%) (Zhang et al. 2017) for SMX in 3 h. In contrast, the nonmetal (e.g., N, C, and S) doping can form 2p electronic states above the valence band (VB) capable of producing efficient charge transfer electronic transition to the 3d CB of TiO_2 and thus providing high photocatalytic activities (Naldoni et al. 2019). Among these, nitrogen and sulfur have provided better and similar band gap narrowing, but the large ionic radius of sulfur requires much higher formation energy, hence nitrogen doping has proved to be more promising for visible-light-driven photocatalysis (Kumar et al. 2019a). For example, in the previous study, the incorporation of nitrogen into the crystalline TiO_2 lattice may modify the electronic band structure of TiO_2, then a new substitutional N 2p band was formed above the O 2p valance band, which narrowed the TiO_2 band gap, and shifted the optical absorption to the visible light region, resulting in a better performance of N-TiO_2@SiO_2@Fe_3O_4 photocatalyst (Kumar et al. 2019a). The results showed that 93% of benzophenone-3 within 5 h and 71% of carbamazepine within 9 h were degraded under visible light. A Ti-coupled N-embedded chicken feather biochar also presented a 90.91% degradation rate of Rhodamine B under visible light after 240 min (Li et al. 2018). The direct contact of Fe_3O_4 and TiO_2 may enhance the visible light response a little, whereas it brings an unfavorable heterojunction, resulting in lower photocatalytic performance. Obviously, the oxidation rate for Rhodamine B degradation (75% in 1 h) using TiO_2-olive pits@Fe_3O_4 is faster than that of Ti-coupled N-embedded chicken feather biochar, due to the presence of olive pit biomass, which can enhance adsorption capacity and serve as a charge acceptor via Ti–O–C bridge and inhibit the transfer of electron/hole charges from TiO_2 to Fe_3O_4 (Djellabi et al. 2019a).

4.4.3 Graphite carbon nitride

Graphitic C_3N_4, as a nonmetal photocatalyst, possesses a comparatively narrower bandgap of ca. 2.7 eV, good thermal chemical stability and cheaper cost than TiO_2. Unfortunately, bulk g-C_3N_4 exhibits poor electronic properties, small specific surface area and low quantum yield due to structural defects of stacking of the layers, and tremendous efforts have been made to improve the photocatalytic efficiency through design strategies, including band-gap engineering, defect control, pore texture tailoring, dimensionality tuning, surface sensitization, heterojunction construction, co-catalyst and nanocarbon loading (Wen et al. 2017). Similarly, biochar can play an important role in enhancing the photocatalytic activity of g-C_3N_4. A simple biochar@g-C_3N_4 composite initially was used to degrade cationic dye, exhibiting a more desirable decolorization rate of 91% for methylene blue than that of C_3N_4 in 3 h, due to enhanced methylene blue adsorption (Pi et al. 2015). It can be found that the cationic dye methylene blue decolorization capacity of biochar@g-C_3N_4 is lower than that of TiO_2-Lignocellulosic Biomass@Fe_3O_4 (Djellabi et al. 2019a) and TiO_2/Fe/Fe_3C-biochar (Mian and Liu 2019). However, biochar@g-C_3N_4 catalyst may be more practical in the application of cationic dye decolorization, due to better visible light absorption. Recently, the antibiotic TC degradation is still a challenge, due to its recalcitrance. It was reported the biochar spheres acted both as a reservoir and a sensitizer in biochar@g-C_3N_4 core–shell photocatalyst to enhance light absorption in nearly the entire wavelength range due to the narrower gap of the sp^2 carbon cluster and large amounts of carbon clusters (Wang et al. 2018b). The core–shell non-metallic photocatalyst exhibited a degradation rate of 55% for TC (10 mg·L^{-1}) in 80 min under visible light irradiation, which was 4 times as high as that of the g-C_3N_4. The degradation of TC using biochar@g-C_3N_4 in photocatalysis system is far below that of biochar-based catalyst using in Fenton-like system. An oxidation biochar supported magnetite particles (OBC-Fe_3O_4) exhibited better catalytic performance for PS activation due to its abundant oxygen-containing groups on the surface and Fe_3O_4 particles, which resulted in 92.3% of TC (20 mg·L^{-1}) removal within 2 h (Pi et al. 2019). Even so, the degradation performance of TC is not good enough, using either the biochar@g-C_3N_4 composite in catalysis system or biochar-based catalysts in the Fenton-like system. To design a photo-Fenton system via taking advantage of photocatalysis and Fenton-like reactions may be a promising way to further enhance the degradation of TC.

4.4.4 Bismuth oxyhalide

As a common semiconductor with a special layered structure, BiOX is composed of [Bi_2O_2] slabs interleaved with double halogen atoms labs, which can effectively separate electrons and holes (Li et al. 2016). However, the inherent large band gaps of BiOCl (∼ 3.4 eV) and BiOBr (∼ 2.6 eV) still restricted their applications in solar conversion, various strategies such as heterojunction formation, doping, interface modification, enhancement in Bi content, inner coupling between different BiOX photocatalysts, use of sensitizers and creation of oxygen vacancies can improve photocatalytic performance (Sharma et al. 2019). Li developed biochar/BiOBr composite photocatalysts, and the visible-light absorption of BiOX catalysts can be exceedingly enhanced by biochar, which mainly stems from the profoundly improved charge separation and delivery efficiency (Li et al. 2016). And the catalysis ability is affected by the mass ratio between biochar and BiOX, and for10% biochar/BiOBr, the degradation efficiency of methyl orange reaches 82% under visible-light irradiation within 2.5 h, which is much higher than that of pure BiOBr. Obviously, the biochar/BiOBr exhibited slightly lower degradation efficiency of methyl orange than that of TiO_2/biochar (Lu et al. 2019), while biochar/BiOBr had a better practical application prospect in decolorization of cationic dyes, due to the wide visible-light adsorption.

4.4.5 Other photocatalysts

Other photocatalysts were also used to couple with biochars. Liu prepared Ag/Ag_3PO_4 support amino-modified biochar composite, which exhibited greatly enhanced photocatalytic performance, and almost 80% amoxicillin was decomposed in 120 min, whereas only 65% with pure Ag_3PO_4 (Liu et al. 2017a). The CdS load activated biomass carbon composite displayed excellent photocatalytic ability toward methyl orange and methylene blue degradation with the efficiency of 97.8% at 60 min and 96.3% at 150 min, respectively (Huang et al. 2018b). $CuWO_4$, a n-type semiconductor, was supported on biochar to construct a Biochar-$CuWO_4$ composite with degradation up to 97% of ciprofloxacin after 90 min of visible light irradiation (Thiruppathi et al. 2020). Besides, the nanocomposites exhibited complete photodegradation of methylene blue and Rhodamine B solutions after 80 min of light irradiation. In a work, an N-modified biochar, with great conductivity and a special 2D sheet platform structure, was used as a platform for supporting Bi_2WO_6, causing a narrower band gap of the composites than that of Bi_2WO_6 (Wang et al. 2020c). The composites exhibited excellent photocatalytic activity for the degradation of

10 mg·L^{-1} Rhodamine B (99.1%, 45 min) and reduction of Cr(VI) (96.7%, 30 min) under visible light irradiation. In conclusion, it could be found that the new biochar-based CdS, $CuWO_4$, Bi_2WO_6 composites can very efficiently (nearly 100% within 2.5 h) degrade cationic dyes, such as Rhodamine B, methyl orange, methylene blue and so on, under visible light, the performance of which is better than that of biochar/BiOX. Compared to conventional TiO_2 or g-C_3N_4 based catalysts, the new catalysts, such as g-MoS_2, $Bi_4Ti_3O_{12}$ based catalysts and so on, have better performance for TC degradation. A porous graphite biochar self-assembled with g-MoS_2 nanosheets is observed to have enhanced visible light harvesting, accelerated charge transfer, efficient carrier's separation, and excellent performance for TC degradation, and more than 40% of the total organic carbon (TOC) could be removed after 60 min under visible light irradiation (Ye et al. 2019). Similarly, the metal doping can further improve photocatalytic performance. Wang reported Ag can be applied as excited electron–hole pairs in biochar quantum-dot/$Bi_4Ti_3O_{12}$ nanosheets by transferring the plasmonic energy from the metal to the semiconductor, and the 2D Ag/carbon quantum dots/bismuth titanate exhibited a high degradation efficiency of almost 90% for TC (10 mg·g^{-1}) under visible-light irradiation after 90 min (Wang et al. 2019b). The surface plasmon resonance of Ag can promote the electron transfer properties of the biochar quantum-dots, meanwhile, it can act as an electron buffer to decrease the recombination rate of the electron hole, and provide a chemical group to enhance the electron transfer and connection.

4.4.6 Heterojunctions

Among these strategies, the construction of heterojunctions has seen a recent explosion of interest due to further improvement in photocatalytic efficiency of biochar coupled single photocatalysts. According to the heterojunction energy band theory, when different semiconductors with the difference in energy band structure are combined, the semiconductors can absorb the radiant energy and be excited to generate electron–hole pairs, and with a heterojunction, the band gap energy can be significantly reduced and therefore light absorption as well as charge transfer will be increased (Wen et al. 2017). Recently, the biochar coupled heterojunction composites were prepared, and exhibited superior photocatalytic performance, due to the narrow band gap, high surface area, broader solar spectrum response and reduced charge carrier recombination. Among oxide-based semiconductors, Cu_2O and CuO as the p-type semiconducting materials have a relatively narrow band gap of 1.8–2.2 eV and 1.2–1.8 eV, respectively. The potential difference in the VB or CB of Cu_2O and CuO could lead to the transference of the electrons on the CuO and Cu_2O CB and the hole from CuO to the VB of Cu_2O, hence 94.12% degradation efficiency of Reactive Orange 29 was obtained by the composite at the initial concentration of 20 mg·L^{-1} after 90 min under UV-B light irradiation (Khataee et al. 2019). By the utilization of g-C_3N_4, polyaniline (PANI), reduced graphene oxide (RGO) and biochar, a Z-scheme photocatalyst g-C_3N_4/ACN/RGO@biochar was synthesized and exhibited a high degradation of 99.7% and 98.4% for 2,4-Dichlorophenoxy acetic acid and ibuprofen (20 mg·L^{-1}) under visible light exposure in 50 min (Kumar et al. 2019b). Similarly, Ag_3PO_4 is a visible light-responsive photocatalyst with a higher quantum efficiency (90%) but susceptible to photo corrosion caused by Ag^+ reduction, which could be solved by constructing Z-scheme heterojunctions with $CoFe_2O_4$, hence a biochar@$CoFe_2O_4$/Ag_3PO_4 Z-scheme composite was prepared, and exhibited the high photocatalytic and mineralization ability of 91.12% and 80.23% for bisphenol under visible-light within 60 min (Zhai et al. 2020). In conclusion, the heterojunctions, especially Z-scheme composite, exhibited higher photocatalytic efficiency than that of biochar coupled single photocatalyst, and the mass ratio between biochar and catalysts significantly affected the performance of the composite. However, the cost of heterojunction photocatalysts is comparatively higher, due to the multistep synthetic process and induction of some precious metals, such as Ag. Consequently, as illustrated in previous studies, the heterojunction photocatalysts may be more applicable to the degradation of toxic and refractory organic contaminants, such as methyl paraben, bisphenol, chlorophenol, ciprofloxacin and so on.

5 Environmental concern of biochar-based catalysts

The excellent performance of biochar-based catalysts applied to water and soil pollution control had accepted widely attention, but potential environmental effects remain largely unexplored and poorly understood. Generally speaking, the potential risk of biochar-based catalysts toward the environment mainly stems from the release of toxic contaminants during the production and application in environmental modifications.

5.1 Impacts of biochar-matrix on environment

The pyrolysis of biomass can generate some toxic contaminants (such as aromatic hydrocarbons, aldehydes and ketone), which are usually highly toxic, with high volatility and low water solubility, particularly high environmental mobility (Raclavska et al. 2018; Shaheen et al. 2019). In general, the pyrolysis at a low temperature can produce biochar with high toxicity owing to

the inadequate combustion (Lyu et al. 2016). Polycyclic aromatic hydrocarbons (PAHs), as a highly toxic persistent organic pollutant, are generated as temperatures approach 1000 °C (Nakajima et al. 2007). PAHs might be toxic to organisms, such as crustaceans, while there is no evidence of the existence of a correlation between PAHs content and the ecotoxicity of biochar to terrestrial flora and fauna (Oleszczuk et al. 2013). This phenomenon might be explained by the synergetic impacts of various contaminants, and the interactions between biochars and contaminants (Liu et al. 2018). The persistent free radicals (PFRs), generated during biomass pyrolysis, could induce the formation of reactive oxygen species, which pose huge agro-environmental and human health risks, due to their half-lives and persistence in both biochar residues and the atmosphere (Odinga et al. 2020). In addition, biochar matrixes may release heavy metals when applied to environmental remediation. For example, the most toxic chemicals dioxins (Hale et al. 2012) and potentially toxic elements, such as Pb, Cd, Cr, Cu, Ni, Zn, and As, have also been detected in biochar (Freddo et al. 2012), which might be released into the environment. A study showed that corn cob biochars inhibited urease activity due to the release of heavy metals and polyaromatic hydrocarbons (Liu et al. 2018). Carbon nanoparticles are difficult to degrade under natural conditions and are harmful to living organisms, and the toxicity mechanism includes oxidative stress response, mechanical damage and effects on biological enzymes (Peng et al. 2020). Moreover, the $^{\cdot}OH$ stemming from biochar and biochar-based catalysts in the aqueous phase may cause significant inhibitory effects on seed germination, seedling root and shoot growth, and the damage of plasma membranes in corn, wheat, and rice (Liao et al. 2014). However, some studies reported that carbon nanoparticles can act as a plant growth inducer causing enhanced plant dry biomass and root/shoot lengths, hence are transpiring as a nanocarbon fertilizer in soil (Vithanage et al. 2017). And the accumulation of carbon nanoparticles in the soil can further modify the balance among plant-toxic metals in soil, thereby enhancing the translocation of heavy metals (loids) into the plant system (Vithanage et al. 2017).

5.2 Impacts of metal nanoparticles of biochar-based catalysts in environment

The preparation process of biochar-based catalysts involves acid/alkali/oxidant, hence might be a pollutant source (Wang et al. 2018e), the toxic elements or metal nanoparticles in biochar-based materials are also non-negligible risks. When applied in environmental modification, these metal compositions may be released into the environment, leading to secondary pollution. Semiconductors such as TiO_2, CuO and ZnO are usually deemed as toxic (Zhang et al. 2018), but iron oxide particles including Fe_3O_4 and Fe_2O_3 are nontoxic or low-toxic matter (Lei et al. 2018). For example, nano-TiO_2 has various negative impacts on the health of a variety of vertebrate animals, and it could cause damage to the cardiac and reproductive systems, and pose a significant threat to the recruitment of broadcast spawning invertebrates (Han et al. 2019). Particle size and shape are important factors affecting toxicity (Suresh et al. 2013). Generally, toxicity increases with the decrease of particle size, and the particles with sharp edges and corners are chemically and biologically reactive, and small spherical particles are more toxic than rod-like particles because they can damage the cell membrane more easily (Zhuang et al. 2017, 2019). Due to the complexity of environmental factors, metal oxide nanoparticles may undergo structural changes, which may further strengthen the toxicity of nanoparticles (Zhang et al. 2018). For example, in the presence of phosphate, ZnO nanoparticles change from uniform spherical particles into larger anomalous porous particles that are more toxic to mammalian cells than the initial nanospheres (Lv et al. 2012). Most of the toxicity studies only focused on the raw nanoparticles, which overlooked the potential harm of nanoparticles under complex natural environmental conditions (Zhuang et al. 2019). In future researches, it is necessary to understand the potential toxicity effects of particles relating to their possible nanostructure changes. The fabrication process of the biochar-based materials should be optimized to improve their stability before and after use, so as to minimize or eliminate the potential release of these toxic contaminants to the environment (Lu et al. 2020).

5.3 The toxicity of reactive intermediates

The intermediates with higher biochemical toxicity than that of the original pollutants might be generated when using biochar-based catalysts to degrade contaminants (Wang et al. 2018d). In most cases, organic pollutants are not completely mineralized by UV-AOPs but are partially oxidized into transformation products (TPs), which could increase the complexity of the water remediation. Although present at low concentrations, TPs might threaten the health of humans, living organisms and eco-systems (Wang et al. 2018d). Fortunately, in most cases, the results are optimistic, the degradation usually causes the reduction of contaminant toxicity (Liang et al. 2021). For example, the toxicity of Cr (III) obtained by the photocatalytic reduction of Cr (VI) is so far below that of Cr (VI). During the process of TC photocatalysis degradation, the acute toxicity of intermediates was lower than that of TC. Worryingly, the bio-accumulative of the TC intermediates increased significantly (Wang et al. 2020e).

6 Conclusions and future perspective

This work reviews recent advances in biochar-based catalyst preparation, application in contaminant removal, and environmental risks. The physicochemical properties of biochar are significantly affected by temperature, and hydrochar with desirable carbon and ash content could be accurately prepared by adjusting the temperature. The choice of the preparation method for catalysts is based on raw materials and desirable catalysts. The enhanced performance of biochar catalysts is mainly attributed to the unique physicochemical properties of biochars, which could be used both as support and electron reservoir, resulting in the increase in adsorption capacity, catalytic active sites and charge separation of catalysts. Nearly complete removal of cationic dyes and hexavalent chromium could be achieved by simple biochar catalysts in photocatalysis, sonocatalytic and redox systems. Biochar heterojunction catalysts are especially suitable for the removal of refractory emerging organic pollutants, due to the better performance but significantly complex preparation process. Emerging organic pollutants could be more efficiently removed by biochar catalysts in a Fenton-like system than those in the other three systems. The toxic contaminants of biochar-matrix, metal nanoparticles of catalysts and intermediates stemming from the reaction process of pollutants are the main risks when using biochar-based catalysts.

Despite considerable progress made in preparation, and application in contaminant removal of biochar-based catalysts, further research still needs to be done due to the complex surface chemistry and heterogeneity of catalysts. In order to choose and design biochar-based catalysts, a deeper understanding is expected on the quantitative correlation and interaction or synergy between feedstock, synthetic process, structure, properties and catalysis performance of catalysts. More importantly, the underlying mechanism is worth studying deeply. Replacement of rare or noble metals with free metals is a promising research area to realize cost efficiency and environmental friendliness. Besides the aforementioned environmental remediation applications, future work should also be devoted to expanding new energy applications of biochar, and biochar-based materials may be a favorable alternative to the expensive carbon materials. We hope that this review not only provides the reader with a good overview of the current advances in biochar-based catalysts for environmental remediation, but also highlights some perspectives remaining in future research.

Author contributions

BY: conceptualization, methodology, writing—original draft. JD: methodology, formal analysis, data curation. YZ: conceptualization, resources, supervision. JW: validation, data curation. CJ: formal analysis, validation. YZ: supervision, funding acquisition, project administration, writing—review and editing. All authors read and approved the final manuscript.

Funding

This work is funded by the National Natural Science Foundation of China under Grant 41671331, the Innovative Approaches Special Project of the Ministry of Science and Technology of China under Grant (2020IM020300), the Beijing–Tianjin–Hebei Collaborative Innovation Promotion Project, China (Z201100006720001) and the National Key Research and Development Program of China under Grant 2016YFA0600103. We want to acknowledge anonymous reviewers for their valuable comments.

Availability of data and materials

All date generated during the current study are available from the corresponding author on reasonable request.

Declarations

Ethics approval and consent to participate

Not applicable.

Competing interests

The authors declare that they have no known competing financial interests or personal relationships that could have appeared to influence the work reported in this paper.

Author details

[1]College of Resource Environment and Tourism, Capital Normal University, Beijing 100048, China. [2]School of Environmental and Safety Engineering, Changzhou University, Changzhou 213164, China.

Received: 12 February 2022 Accepted: 27 June 2022
Published online: 29 August 2022

References

Afzal M, Zu P, Zhang C, Guan J, Song C, Sun X, Wang S (2022) Sonocatalytic degradation of ciprofloxacin using hydrogel beads of TiO_2 incorporated biochar and chitosan. J Hazard Mater 434:128879. https://doi.org/10.1016/j.jhazmat.2022.128879

Ahmaruzzaman M (2021) Biochar based nanocomposites for photocatalytic degradation of emerging organic pollutants from water and wastewater. Mater Res Bull. https://doi.org/10.1016/j.materresbull.2021.111262

Ahmed M, Hameed B (2020) Insight into the co-pyrolysis of different blended feedstocks to biochar for the adsorption of organic and inorganic pollutants: a review. J Clean Prod. https://doi.org/10.1016/j.jclepro.2020.121762

Aller M (2016) Biochar properties: transport, fate, and impact. Crit Rev Environ Sci Technol 46(14–15):1183–1296. https://doi.org/10.1080/10643389.2016.1212368

Baig SA, Lou Z, Hayat MT, Fu R, Liu Y, Xu X (2016) Characterization of magnetic biochar amended with silicon dioxide prepared at high temperature calcination. Mater Sci-Poland 34(3):597–604. https://doi.org/10.1515/msp-2016-0112

Bolan N, Hoang SA, Beiyuan J, Gupta S, Hou D, Karakoti A, Joseph S, Jung S, Kim K-H, Kirkham MB, Kua HW, Kumar M, Kwon EE, Ok YS, Perera V, Rinklebe J, Shaheen SM, Sarkar B, Sarmah AK, Singh BP, Singh G, Tsang DCW, Vikrant K, Vithanage M, Vinu A, Wang H, Wijesekara H, Yan Y, Younis SA, Van Zwieten L (2022) Multifunctional applications of biochar beyond carbon storage. Int Mater Rev 67(2):150–200. https://doi.org/10.1080/09506608.2021.1922047

Cha JS, Park SH, Jung SC, Ryu C, Jeon JK, Shin MC, Park YK (2016) Production and utilization of biochar: a review. J Ind Eng Chem 40:1–15. https://doi.org/10.1016/j.jiec.2016.06.002

Chandra S, Bhattacharya J (2019) Influence of temperature and duration of pyrolysis on the property heterogeneity of rice straw biochar and optimization of pyrolysis conditions for its application in soils. J Clean Prod 215:1123–1139. https://doi.org/10.1016/j.jclepro.2019.01.079

Chen XB, Shen SH, Guo LJ, Mao SS (2010) Semiconductor-based photocatalytic hydrogen generation. Chem Rev 110(11):6503–6570. https://doi.org/10.1021/cr1001645

Chen Z, Xiao X, Chen B, Zhu L (2015) Quantification of chemical states, dissociation constants and contents of oxygen-containing groups on the surface of biochars produced at different temperatures. Environ Sci Technol 49(1):309–317. https://doi.org/10.1021/es5043468

Chen N, Huang YH, Hou XJ, Ai ZH, Zhang LZ (2017) Photochemistry of hydrochar: reactive oxygen species generation and sulfadimidine degradation. Environ Sci Technol 51(19):11278–11287. https://doi.org/10.1021/acs.est.7b02740

Chen B, Yang Z, Ma G, Kong D, Xiong W, Wang J, Zhu Y, Xia Y (2018) Heteroatom-doped porous carbons with enhanced carbon dioxide uptake and excellent methylene blue adsorption capacities. Microporous Mesoporous Mater 257:1–8. https://doi.org/10.1016/j.micromeso.2017.08.026

Chen MX, Dai YZ, Guo J, Yang HT, Liu DN, Zhai YL (2019a) Solvothermal synthesis of biochar@$ZnFe_2O_4$/BiOBr Z-scheme heterojunction for efficient photocatalytic ciprofloxacin degradation under visible light. Appl Surf Sci 493:1361–1367. https://doi.org/10.1016/j.apsusc.2019.04.160

Chen W, Meng J, Han X, Lan Y, Zhang W (2019b) Past, present, and future of biochar. Biochar 1(1):75–87. https://doi.org/10.1007/s42773-019-00008-3

Chen W, Fang Y, Li K, Chen Z, Xia M, Gong M, Chen Y, Yang H, Tu X, Chen H (2020) Bamboo wastes catalytic pyrolysis with N-doped biochar catalyst for phenols products. Appl Energy. https://doi.org/10.1016/j.apenergy.2019.114242

Cheng F, Li X (2018) Preparation and application of biochar-based catalysts for biofuel production. Catalysts. https://doi.org/10.3390/catal8090346

Cho DW, Yoon K, Ahn Y, Su YQ, Tsang DCW, Hou DY, Ok YS, Son H (2019) Fabrication and environmental applications of multifunctional mixed metal-biochar composites (MMBC) from red mud and lignin wastes. J Hazard Mater 374:412–419. https://doi.org/10.1016/j.jhazmat.2019.04.071

Cui W, Xu Y, Luo G, Zhang QZ, Li ZH, Zhang SB (2021) Enhanced mercury removal performance of Cu-Fe binary oxide sorbents modified by non-thermal plasma. Chem Eng J. https://doi.org/10.1016/j.cej.2021.131851

Das S, Ghosh G, Avasthe R, Sinha K (2021) Compositional heterogeneity of different biochar: effect of pyrolysis temperature and feedstocks. J Environ Manage. https://doi.org/10.1016/j.jenvman.2020.111501

De Bhowmick G, Sarmah AK, Sen R (2018) Production and characterization of a value added biochar mix using seaweed, rice husk and pine sawdust: a parametric study. J Clean Prod 200:641–656. https://doi.org/10.1016/j.jclepro.2018.08.002

Ding X, Xiao D, Ji L, Jin D, Dai K, Yang ZX, Wang SY, Chen H (2018) Simple fabrication of Fe_3O_4/C/g-C_3N_4 two-dimensional composite by hydrothermal carbonization approach with enhanced photocatalytic performance under visible light. Catal Sci Technol 8(14):3484–3492. https://doi.org/10.1039/c8cy00698a

Ding DH, Yang SJ, Qian XY, Chen LW, Cai TM (2020) Nitrogen-doping positively whilst sulfur-doping negatively affect the catalytic activity of biochar for the degradation of organic contaminant. Appl Catal B 263:15. https://doi.org/10.1016/j.apcatb.2019.118348

Djellabi R, Yang B, Sharif HMA, Zhang JJ, Ali J, Zhao X (2019a) Sustainable and easy recoverable magnetic TiO_2-Lignocellulosic Biomass@Fe_3O_4 for solar photocatalytic water remediation. J Clean Prod 233:841–847. https://doi.org/10.1016/j.jclepro.2019.06.125

Djellabi R, Yang B, Wang Y, Cui XQ, Zhao X (2019b) Carbonaceous biomass-titania composites with Ti-O-C bonding bridge for efficient photocatalytic reduction of Cr(VI) under narrow visible light. Chem Eng J 366:172–180. https://doi.org/10.1016/j.cej.2019.02.035

Dong XL, Ma LQ, Gress J, Harris W, Li YC (2014) Enhanced Cr(VI) reduction and As(III) oxidation in ice phase: important role of dissolved organic matter from biochar. J Hazard Mater 267:62–70. https://doi.org/10.1016/j.jhazmat.2013.12.027

Du WY, Zhang QZ, Shang YN, Wang W, Li Q, Yue QY, Gao BY, Xu X (2020) Sulfate saturated biosorbent-derived Co-S@NC nanoarchitecture as an efficient catalyst for peroxymonosulfate activation. Appl Catal B. https://doi.org/10.1016/j.apcatb.2019.118302

El-Naggar A, Lee M-H, Hur J, Lee YH, Igalavithana AD, Shaheen SM, Ryu C, Rinklebe J, Tsang DCW, Ok YS (2020) Biochar-induced metal immobilization and soil biogeochemical process: an integrated mechanistic approach. Sci Total Environ. https://doi.org/10.1016/j.scitotenv.2019.134112

Fakayode O, Aboagarib E, Zhou C, Ma HL (2020) Co-pyrolysis of lignocellulosic and macroalgae biomasses for the production of biochar—a review. Bioresour Technol. https://doi.org/10.1016/j.biortech.2019.122408

Fang GD, Zhu CY, Dionysiou DD, Gao J, Zhou DM (2015) Mechanism of hydroxyl radical generation from biochar suspensions: implications to diethyl phthalate degradation. Bioresour Technol 176:210–217. https://doi.org/10.1016/j.biortech.2014.11.032

Fang G, Liu C, Wang Y, Dionysiou DD, Zhou D (2017) Photogeneration of reactive oxygen species from biochar suspension for diethyl phthalate degradation. Appl Catal B 214:34–45. https://doi.org/10.1016/j.apcatb.2017.05.036

Fernandez-Sanroman A, Lama G, Pazos M, Rosales E, Angeles Sanroman M (2021) Bridging the gap to hydrochar production and its application into frameworks of bioenergy, environmental and biocatalysis areas. Bioresour Technol 320:124399. https://doi.org/10.1016/j.biortech.2020.124399

Foong SY, Liew RK, Yang YF, Cheng YW, Yek PNY, Mahari WAW, Lee XY, Han CS, Vo DVN, Le QV, Aghbashlo M, Tabatabaei M, Sonne C, Peng WX, Lam SS (2020) Valorization of biomass waste to engineered activated biochar by microwave pyrolysis: progress, challenges, and future directions. Chem Eng J 389:20. https://doi.org/10.1016/j.cej.2020.124401

Freddo A, Cai C, Reid BJ (2012) Environmental contextualisation of potential toxic elements and polycyclic aromatic hydrocarbons in biochar. Environ Pollut 171:18–24. https://doi.org/10.1016/j.envPol.2012.07.009

Fredriksson H, Lancee R, Thune P, Veringa HJ, Niemantsverdriet JW (2013) Olivine as tar removal catalyst in biomass gasification: catalyst dynamics under model conditions. Appl Catal B 130:168–177. https://doi.org/10.1016/j.apcatb.2012.10.017

Fu D, Chen Z, Xia D, Shen L, Wang YP, Li QBA (2017) A novel solid digestate-derived biochar-Cu NP composite activating H_2O_2 system for simultaneous adsorption and degradation of tetracycline. Environ Pollut 221:301–310. https://doi.org/10.1016/j.envpol.2016.11.078

Gale M, Nguyen T, Moreno M, Gilliard-AbdulAzir KL (2021) Physiochemical properties of biochar and activated carbon from biomass residue: influence of process conditions to adsorbent properties. ACS Omega 6(15):10224–10233. https://doi.org/10.1021/acsomega.1c00530

Ghanim BM, Pandey DS, Kwapinski W, Leahy JJ (2016) Hydrothermal carbonisation of poultry litter: effects of treatment temperature and residence time on yields and chemical properties of hydrochars. Bioresour Technol 216:373–380. https://doi.org/10.1016/j.biortech.2016.05.087

Gholami P, Dinpazhoh L, Khataee A, Orooji Y (2019a) Sonocatalytic activity of biochar-supported ZnO nanorods in degradation of gemifloxacin: synergy study, effect of parameters and phytotoxicity evaluation. Ultrason Sonochem 55:44–56. https://doi.org/10.1016/j.ultsonch.2019.03.001

Gholami P, Khataee A, Soltani RDC, Bhatnagar A (2019b) A review on carbon-based materials for heterogeneous sonocatalysis: fundamentals, properties and applications. Ultrason Sonochem. https://doi.org/10.1016/j.ultsonch.2019.104681

Gholami P, Dinpazhoh L, Khataee A, Hassani A, Bhatnagar A (2020a) Facile hydrothermal synthesis of novel Fe-Cu layered double hydroxide/biochar nanocomposite with enhanced sonocatalytic activity for degradation of cefazolin sodium. J Hazard Mater. https://doi.org/10.1016/j.jhazmat.2019.120742

Gholami P, Khataee A, Soltani R, Dinpazhoh L, Bhatnagar A (2020b) Photocatalytic degradation of gemifloxacin antibiotic using Zn-Co-LDH@biochar nanocomposite. J Hazard Mater. https://doi.org/10.1016/j.jhazmat.2019.121070

Gholizadeh M, Hu X, Liu Q (2021) Progress of using biochar as a catalyst in thermal conversion of biomass. Rev Chem Eng 37(2):229–258. https://doi.org/10.1515/revce-2018-0070

Hadiya V, Popat K, Vyas S, Varjani S, Vithanage M, Kumar Gupta V, Nunez Delgado A, Zhou Y, Loke Show P, Bilal M, Zhang Z, Sillanpaa M, Sabyasachi Mohanty S, Patel Z (2022) Biochar production with amelioration of

microwave-assisted pyrolysis: current scenario, drawbacks and perspectives. Bioresour Technol 355:127303–127303. https://doi.org/10.1016/j.biortech.2022.127303

Haeldermans T, Claesen J, Maggen J, Carleer R, Yperman J, Adriaensens P, Samyn P, Vandamme D, Cuypers A, Vanreppelen K, Schreurs S (2019) Microwave assisted and conventional pyrolysis of MDF—characterization of the produced biochars. J Anal Appl Pyrolysis 138:218–230. https://doi.org/10.1016/j.jaap.2018.12.027

Hale SE, Lehmann J, Rutherford D, Zimmerman AR, Bachmann RT, Shitumbanuma V, O'Toole A, Sundqvist KL, Arp HPH, Cornelissen G (2012) Quantifying the total and bioavailable polycyclic aromatic hydrocarbons and dioxins in biochars. Environ Sci Technol 46(5):2830–2838. https://doi.org/10.1021/es203984k

Han J, Kim H (2008) The reduction and control technology of tar during biomass gasification/pyrolysis: an overview. Renew Sustain Energy Rev 12(2):397–416. https://doi.org/10.1016/j.rser.2006.07.015

Han Y, Shi W, Rong JH, Zha SJ, Guan XF, Sun HX, Liu GX (2019) Exposure to waterborne $nTiO_2$ reduces fertilization success and increases polyspermy in a bivalve mollusc: a threat to population recruitment. Environ Sci Technol 53(21):12754–12763. https://doi.org/10.1021/acs.est.9b03675

Ho SH, Chen YD, Li RX, Zhang CF, Ge YM, Cao GL, Ma M, Duan XG, Wang SB, Ren NQ (2019) N-doped graphitic biochars from C-phycocyanin extracted Spirulina residue for catalytic persulfate activation toward nonradical disinfection and organic oxidation. Water Res 159:77–86. https://doi.org/10.1016/j.watres.2019.05.008

Hu B, Ai Y, Jin J, Hayat T, Alsaedi A, Zhuang L, Wang X (2020) Efficient elimination of organic and inorganic pollutants by biochar and biochar-based materials. Biochar 2(1):47–64. https://doi.org/10.1007/s42773-020-00044-4

Huang DL, Wang Y, Zhang C, Zeng GM, Lai C, Wan J, Qin L, Zeng Y (2016) Influence of morphological and chemical features of biochar on hydrogen peroxide activation: implications on sulfamethazine degradation. RSC Adv 6(77):73186–73196. https://doi.org/10.1039/c6ra11850j

Huang BC, Jiang J, Huang GX, Yu HQ (2018a) Sludge biochar-based catalysts for improved pollutant degradation by activating peroxymonosulfate. J Mater Chem A 6(19):8978–8985. https://doi.org/10.1039/c8ta02282h

Huang HB, Wang Y, Jiao WB, Cai FY, Shen M, Zhou SG, Cao HL, Lu J, Cao R (2018b) Lotus-leaf-derived activated-carbon-supported nano-CdS as energy-efficient photocatalysts under visible irradiation. ACS Sustain Chem Eng 6(6):7871–7879. https://doi.org/10.1021/acssuschemeng.8b01021

Huang P, Zhang P, Wang C, Tang J, Sun H (2022) Enhancement of persulfate activation by Fe-biochar composites: synergism of Fe and N-doped biochar. Appl Catal B. https://doi.org/10.1016/j.apcatb.2021.120926

Issaka E, Fapohunda F, Amu Darko J, Yeboah L, Yakubu S, Varjani S, Ali N, Bilal M (2022) Biochar-based composites for remediation of polluted wastewater and soil environments: challenges and prospects. Chemosphere. https://doi.org/10.1016/j.chemosphere.2022.134163

Jiao Y, Li D, Wang M, Gong T, Sun M, Yang T (2021) A scientometric review of biochar preparation research from 2006 to 2019. Biochar 3(3):283–298. https://doi.org/10.1007/s42773-021-00091-5

Jung KW, Lee SY, Lee YJ, Choi JW (2019) Ultrasound-assisted heterogeneous Fenton-like process for bisphenol A removal at neutral pH using hierarchically structured manganese dioxide/biochar nanocomposites as catalysts. Ultrason Sonochem 57:22–28. https://doi.org/10.1016/j.ultsonch.2019.04.039

Kabir G, Hameed BH (2017) Recent progress on catalytic pyrolysis of lignocellulosic biomass to high-grade bio-oil and bio-chemicals. Renew Sustain Energy Rev 70:945–967. https://doi.org/10.1016/j.rser.2016.12.001

Kasera N, Kolar P, Hall S (2022) Nitrogen-doped biochars as adsorbents for mitigation of heavy metals and organics from water: a review. Biochar. https://doi.org/10.1007/s42773-022-00145-2

Khan TA, Saud AS, Jamari SS, Ab Rahim MH, Park JW, Kim HJ (2019) Hydrothermal carbonization of lignocellulosic biomass for carbon rich material preparation: a review. Biomass Bioenergy. https://doi.org/10.1016/j.biombioe.2019.105384

Khataee A, Kayan B, Gholami P, Kalderis D, Akay S (2017a) Sonocatalytic degradation of an anthraquinone dye using TiO_2-biochar nanocomposite. Ultrason Sonochem 39:120–128. https://doi.org/10.1016/j.ultsonch.2017.04.018

Khataee A, Kayan B, Gholami P, Kalderis D, Akay S, Dinpazhoh L (2017b) Sonocatalytic degradation of Reactive Yellow 39 using synthesized ZrO_2 nanoparticles on biochar. Ultrason Sonochem 39:540–549. https://doi.org/10.1016/j.ultsonch.2017.05.023

Khataee A, Gholami P, Kalderis D, Pachatouridou E, Konsolakis M (2018) Preparation of novel CeO_2-biochar nanocomposite for sonocatalytic degradation of a textile dye. Ultrason Sonochem 41:503–513. https://doi.org/10.1016/j.ultsonch.2017.10.013

Khataee A, Kalderis D, Gholami P, Fazli A, Moschogiannaki M, Binas V, Lykaki M, Konsolakis M (2019) Cu_2O-CuO@biochar composite: synthesis, characterization and its efficient photocatalytic performance. Appl Surf Sci. https://doi.org/10.1016/j.apsusc.2019.143846

Kim J, Park B, Son Y, Khim J (2018) Peat moss-derived biochar for sonocatalytic applications. Ultrason Sonochem 42:26–30. https://doi.org/10.1016/j.ultsonch.2017.11.005

Kim JY, Oh S, Park YK (2020) Overview of biochar production from preservative-treated wood with detailed analysis of biochar characteristics, heavy metals behaviors, and their ecotoxicity. J Hazard Mater 384:121356. https://doi.org/10.1016/j.jhazmat.2019.121356

Kumar A, Kumar A, Sharma G, Naushad M, Stadler FJ, Ghfar AA, Dhiman P, Saini RV (2017) Sustainable nano-hybrids of magnetic biochar supported g-C_3N_4/$FeVO_4$ for solar powered degradation of noxious pollutants Synergism of adsorption, photocatalysis & photo-ozonation. J Clean Prod 165:431–451. https://doi.org/10.1016/j.jclepro.2017.07.117

Kumar A, Kumar A, Sharma G, Al-Muhtaseb AH, Naushad M, Ghfar AA, Guo CS, Stadler FJ (2018) Biochar-templated g-C_3N_4/$Bi_2O_2CO_3$/$CoFe_2O_4$ nano-assembly for visible and solar assisted photo-degradation of paraquat, nitrophenol reduction and CO_2 conversion. Chem Eng J 339:393–410. https://doi.org/10.1016/j.cej.2018.01.105

Kumar A, Khan M, Fang LP, Lo IMC (2019a) Visible-light-driven N-TiO_2@SiO_2@Fe_3O_4 magnetic nanophotocatalysts: synthesis, characterization, and photocatalytic degradation of PPCPs. J Hazard Mater 370:108–116. https://doi.org/10.1016/j.jhazmat.2017.07.048

Kumar A, Sharma G, Naushad M, Al-Muhtaseb AH, Kumar A, Hira I, Ahamad T, Ghfar AA, Stadler FJ (2019b) Visible photodegradation of ibuprofen and 2,4-D in simulated waste water using sustainable metal free-hybrids based on carbon nitride and biochar. J Environ Manage 231:1164–1175. https://doi.org/10.1016/j.jenvman.2018.11.015

Kwon G, Cho D-W, Tsang DCW, Kwon EE, Song H (2018) One step fabrication of carbon supported cobalt pentlandite (Co_9S_8) via the thermolysis of lignin and Co_3O_4. J CO2 Util 27:196–203. https://doi.org/10.1016/j.jcou.2018.07.016

Kwon G, Bhatnagar A, Wang H, Kwon EE, Song H (2020) A review of recent advancements in utilization of biomass and industrial wastes into engineered biochar. J Hazard Mater. https://doi.org/10.1016/j.jhazmat.2020.123242

Kwon G, Cho DW, Jang H, Lam SS, Song H (2022) Synergistic effects of blending seafood wastes as Co-pyrolysis feedstock on syngas production and biochar properties. Chem Eng J. https://doi.org/10.1016/j.cej.2021.132487

Lee XJ, Ong HC, Gan YY, Chen W-H, Mahlia TMI (2020) State of art review on conventional and advanced pyrolysis of macroalgae and microalgae for biochar, bio-oil and bio-syngas production. Energy Convers Manag. https://doi.org/10.1016/j.enconman.2020.112707

Lei C, Sun YQ, Tsang DCW, Lin DH (2018) Environmental transformations and ecological effects of iron-based nanoparticles. Environ Pollut 232:10–30. https://doi.org/10.1016/j.envpol.2017.09.052

Li M, Huang HW, Yu SX, Tian N, Dong F, Du X, Zhang YH (2016) Simultaneously promoting charge separation and photoabsorption of BiOX (X = Cl, Br) for efficient visible-light photocatalysis and photosensitization by compositing low-cost biochar. Appl Surf Sci 386:285–295. https://doi.org/10.1016/j.apsusc.2016.05.171

Li HQ, Hu JT, Zhou X, Li X, Wang XJ (2018) An investigation of the biochar-based visible-light photocatalyst via a self-assembly strategy. J Environ Manage 217:175–182. https://doi.org/10.1016/j.jenvman.2018.03.083

Li S, Shao L, Zhang H, He P, Lu F (2020) Quantifying the contributions of surface area and redox-active moieties to electron exchange capacities of biochar. J Hazard Mater 394:122541. https://doi.org/10.1016/j.jhazmat.2020.122541

Li Y, Yu H, Liu L, Yu H (2021) Application of co-pyrolysis biochar for the adsorption and immobilization of heavy metals in contaminated

environmental substrates. J Hazard Mater. https://doi.org/10.1016/j.jhazmat.2021.126655
Li X, Jia Y, Zhang J, Qin Y, Wu Y, Zhou M, Sun J (2022) Efficient removal of tetracycline by H_2O_2 activated with iron-doped biochar: performance, mechanism, and degradation pathways. Chin Chem Lett 33(4):2105–2110. https://doi.org/10.1016/j.cclet.2021.08.054
Liang L, Xi F, Tan W, Meng X, Hu B, Wang X (2021) Review of organic and inorganic pollutants removal by biochar and biochar-based composites. Biochar 3(3):255–281. https://doi.org/10.1007/s42773-021-00101-6
Liao SH, Pan B, Li H, Zhang D, Xing BS (2014) Detecting free radicals in biochars and determining their ability to inhibit the germination and growth of corn, wheat and rice seedlings. Environ Sci Technol 48(15):8581–8587. https://doi.org/10.1021/es404250a
Liu WJ, Ling LL, Wang YY, He H, He YR, Yu HQ, Jiang H (2016) One-pot high yield synthesis of Ag nanoparticle-embedded biochar hybrid materials from waste biomass for catalytic Cr(VI) reduction. Environ Sci Nano 3(4):745–753. https://doi.org/10.1039/c6en00109b
Liu XQ, Chen WJ, Jiang H (2017a) Facile synthesis of Ag/Ag_3PO_4/AMB composite with improved photocatalytic performance. Chem Eng J 308:889–896. https://doi.org/10.1016/j.cej.2016.09.125
Liu Y, Yao S, Wang Y, Lu H, Brar SK, Yang S (2017b) Bio- and hydrochars from rice straw and pig manure: inter-comparison. Bioresour Technol 235:332–337. https://doi.org/10.1016/j.biortech.2017.03.103
Liu Y, Dai QY, Jin XQ, Dong XD, Peng J, Wu M, Liang N, Pan B, Xing BS (2018) Negative impacts of biochars on urease activity: High pH, heavy metals, polycyclic aromatic hydrocarbons, or free radicals? Environ Sci Technol 52(21):12740–12747. https://doi.org/10.1021/acs.est.8b00672
Liu C, Chen LW, Ding DH, Cai TM (2019a) From rice straw to magnetically recoverable nitrogen doped biochar: efficient activation of peroxymonosulfate for the degradation of metolachlor. Appl Catal B 254:312–320. https://doi.org/10.1016/j.apcatb.2019a.05.014
Liu CH, Chu WY, Li H, Boyd SA, Teppen BJ, Mao JD, Lehmann J, Zhang W (2019b) Quantification and characterization of dissolved organic carbon from biochars. Geoderma 335:161–169. https://doi.org/10.1016/j.geoderma.2018.08.019
Liu Y, Li Y, Huang J, Zhang YL, Ruan ZH, Hu T, Wang JJ, Li WY, Hu HJ, Jiang GB (2019c) An advanced sot-gel strategy for enhancing interfacial reactivity of iron oxide nanoparticles on rosin biochar substrate to remove Cr(VI). Sci Total Environ 690:438–446. https://doi.org/10.1016/j.scitotenv.2019.07.021
Liu B, Guo W, Wang H, Si Q, Zhao Q, Luo H, Ren N (2020a) Activation of peroxymonosulfate by cobalt-impregnated biochar for atrazine degradation: the pivotal roles of persistent free radicals and ecotoxicity assessment. J Hazard Mater. https://doi.org/10.1016/j.jhazmat.2020.122768
Liu B, Guo W, Wang H, Si Q, Zhao Q, Luo H, Ren N (2020b) B-doped graphitic porous biochar with enhanced surface affinity and electron transfer for efficient peroxydisulfate activation. Chem Eng J. https://doi.org/10.1016/j.cej.2020.125119
Liu J, Luo K, Li X, Yang Q, Wang D, Wu Y, Chen Z, Huang X, Pi Z, Du W, Guan Z (2020c) The biochar-supported iron-copper bimetallic composite activating oxygen system for simultaneous adsorption and degradation of tetracycline. Chem Eng J. https://doi.org/10.1016/j.cej.2020.126039
Lopes R, Astruc D (2021) Biochar as a support for nanocatalysts and other reagents: recent advances and applications. Coord Chem Rev 426(1):213585. https://doi.org/10.1016/j.ccr.2020.213585
Low Y, Yee K (2021) A review on lignocellulosic biomass waste into biochar-derived catalyst: current conversion techniques, sustainable applications and challenges. Biomass Bioenergy. https://doi.org/10.1016/j.biombioe.2021.106245
Lu LL, Shan R, Shi YY, Wang SX, Yuan HR (2019) A novel TiO_2/biochar composite catalysts for photocatalytic degradation of methyl orange. Chemosphere 222:391–398. https://doi.org/10.1016/j.chemosphere.2019.01.132
Lu L, Yu W, Wang Y, Zhang K, Zhu X, Zhang Y, Wu Y, Ullah H, Xiao X, Chen B (2020) Application of biochar-based materials in environmental remediation: from multi-level structures to specific devices. Biochar 2(1):1–31. https://doi.org/10.1007/s42773-020-00041-7
Luo X, Shen M, Liu J, Ma Y, Gong B, Liu H, Huang Z (2021) Resource utilization of piggery sludge to prepare recyclable magnetic biochar for highly efficient degradation of tetracycline through peroxymonosulfate activation. J Clean Prod. https://doi.org/10.1016/j.jclepro.2021.126372
Lv JT, Zhang SZ, Luo L, Han W, Zhang J, Yang K, Christie P (2012) Dissolution and microstructural transformation of ZnO nanoparticles under the influence of phosphate. Environ Sci Technol 46(13):7215–7221. https://doi.org/10.1021/es301027a
Lyu HH, He YH, Tang JC, Hecker M, Liu QL, Jones PD, Codling G, Giesy JP (2016) Effect of pyrolysis temperature on potential toxicity of biochar if applied to the environment. Environ Pollut 218:1–7. https://doi.org/10.1016/j.envpol.2016.08.014
Lyu H, Zhang Q, Shen B (2020) Application of biochar and its composites in catalysis. Chemosphere 240:124842. https://doi.org/10.1016/j.chemosphere.2019.124842
Mao QM, Zhou YY, Yang YA, Zhang JC, Liang LF, Wang HL, Luo S, Luo L, Jeyakumar P, Ok YS, Rizwan M (2019) Experimental and theoretical aspects of biochar-supported nanoscale zero-valent iron activating H_2O_2 for ciprofloxacin removal from aqueous solution. J Hazard Mater. https://doi.org/10.1016/j.jhazmat.2019.120848
Men QY, Wang T, Ma CC, Yang LL, Liu Y, Huo PW, Yan YS (2019) In-suit preparation of CdSe quantum dots/porous channel biochar for improving photocatalytic activity for degradation of tetracycline. J Taiwan Inst Chem Eng 99:180–192. https://doi.org/10.1016/j.jtice.2019.03.019
Meyer S, Glaser B, Quicker P (2011) Technical, economical, and climate-related aspects of biochar production technologies: a literature review. Environ Sci Technol 45(22):9473–9483. https://doi.org/10.1021/es201792c
Mian MM, Liu G (2018) Recent progress in biochar-supported photocatalysts: synthesis, role of biochar, and applications. RSC Adv 8(26):14237–14248. https://doi.org/10.1039/c8ra02258e
Mian MM, Liu GJ (2019) Sewage sludge-derived TiO_2/Fe/Fe_3C-biochar composite as an efficient heterogeneous catalyst for degradation of methylene blue. Chemosphere 215:101–114. https://doi.org/10.1016/j.chemosphere.2018.10.027
Murtaza G, Ditta A, Ullah N, Usman M, Ahmed Z (2021) Biochar for the management of nutrient impoverished and metal contaminated soils: preparation, applications, and prospects. J Soil Sci Plant Nutr 21(3):2191–2213. https://doi.org/10.1007/s42729-021-00514-z
Nakajima D, Nagame S, Kuramochi H, Sugita K, Kageyama S, Shiozaki T, Takemura T, Shiraishi F, Goto S (2007) Polycyclic aromatic hydrocarbon generation behavior in the process of carbonization of wood. Bull Environ Contam Toxicol 79(2):221–225. https://doi.org/10.1007/s00128-007-9177-8
Naldoni A, Altomare M, Zoppellaro G, Liu N, Kment S, Zboril R, Schmuki P (2019) Photocatalysis with reduced TiO_2: from black TiO_2 to cocatalyst-free hydrogen production. ACS Catal 9(1):345–364. https://doi.org/10.1021/acscatal.8b04068
Nizamuddin S, Baloch HA, Griffin GJ, Mubarak NM, Bhutto AW, Abro R, Mazari SA, Ali BS (2017) An overview of effect of process parameters on hydrothermal carbonization of biomass. Renew Sustain Energy Rev 73:1289–1299. https://doi.org/10.1016/j.rser.2016.12.122
Norgate T, Langberg D (2009) Environmental and economic aspects of charcoal use in steelmaking. Isij Int 49(4):587–595. https://doi.org/10.2355/isijinternational.49.587
Odinga ES, Waigi MG, Gudda FO, Wang J, Yang B, Hu X, Li S, Gao Y (2020) Occurrence, formation, environmental fate and risks of environmentally persistent free radicals in biochars. Environ Int 134:105172. https://doi.org/10.1016/j.envint.2019.105172
Oh SY, Seo YD, Ryu KS, Park DJ, Lee SH (2017) Redox and catalytic properties of biochar-coated zero-valent iron for the removal of nitro explosives and halogenated phenols. Environ Sci Process Impacts 19(5):711–719. https://doi.org/10.1039/c7em00035a
Oleszczuk P, Josko I, Kusmierz M (2013) Biochar properties regarding to contaminants content and ecotoxicological assessment. J Hazard Mater 260:375–382. https://doi.org/10.1016/j.jhazmat.2013.05.044
Pacheco Antero RV, Fonseca Alves AC, de Oliveira SB, Ojala SA, Brum SS (2020) Challenges and alternatives for the adequacy of hydrothermal carbonization of lignocellulosic biomass in cleaner production systems: a review. J Clean Prod 252:119899. https://doi.org/10.1016/j.jclepro.2019.119899
Pan X, Gu Z, Chen W, Li Q (2021) Preparation of biochar and biochar composites and their application in a Fenton-like process for wastewater decontamination: a review. Sci Total Environ. https://doi.org/10.1016/j.scitotenv.2020.142104

Panwar N, Pawar A (2022) Influence of activation conditions on the physicochemical properties of activated biochar: a review. Biomass Convers Biorefin 12(3):925–947. https://doi.org/10.1007/s13399-020-00870-3
Parmar A, Nema PK, Agarwal T (2014) Biochar production from agro-food industry residues: a sustainable approach for soil and environmental management. Curr Sci 107(10):1673–1682
Peng XM, Wang M, Hu FP, Qiu FX, Dai HL, Cao Z (2019) Facile fabrication of hollow biochar carbon-doped TiO_2/CuO composites for the photocatalytic degradation of ammonia nitrogen from aqueous solution. J Alloys Compd 770:1055–1063. https://doi.org/10.1016/j.jallcom.2018.08.207
Peng Z, Liu XJ, Zhang W, Zeng ZT, Liu ZF, Zhang C, Liu Y, Shao BB, Liang QH, Tang WW, Yuan XZ (2020) Advances in the application, toxicity and degradation of carbon nanomaterials in environment: a review. Environ Int 134:14. https://doi.org/10.1016/j.envint.2019.105298
Pi L, Jiang R, Zhou WC, Zhu H, Xiao W, Wang DH, Mao XH (2015) g-C_3N_4 Modified biochar as an adsorptive and photocatalytic material for decontamination of aqueous organic pollutants. Appl Surf Sci 358:231–239. https://doi.org/10.1016/j.apsusc.2015.08.176
Pi Z, Li X, Wang D, Xu Q, Tao Z, Huang X, Yao F, Wu Y, He L, Yang Q (2019) Persulfate activation by oxidation biochar supported magnetite particles for tetracycline removal: performance and degradation pathway. J Clean Prod 235:1103–1115. https://doi.org/10.1016/j.jclepro.2019.07.037
Qin JL, Chen QC, Sun MX, Sun P, Shen GQ (2017) Pyrolysis temperature-induced changes in the catalytic characteristics of rice husk-derived biochar during 1,3-dichloropropene degradation. Chem Eng J 330:804–812. https://doi.org/10.1016/j.cej.2017.08.013
Raclavska H, Ruzickova J, Skrobankova H, Koval S, Kucbel M, Raclavsky K, Svedova B, Pavlik P, Juchelkova D (2018) Possibilities of the utilization of char from the pyrolysis of tetrapak. J Environ Manage 219:231–238. https://doi.org/10.1016/j.jenvman.2018.05.002
Raheem A, He Q, Ding L, Dastyar W, Yu G (2022) Evaluating performance of pyrolysis and gasification processes of agriculture residues-derived hydrochar: effect of hydrothermal carbonization. J Clean Prod. https://doi.org/10.1016/j.jclepro.2022.130578
Sahoo D, Remya N (2020) Influence of operating parameters on the microwave pyrolysis of rice husk: biochar yield, energy yield, and property of biochar. Biomass Convers Biorefin. https://doi.org/10.1007/s13399-020-00914-8
Saqib U, Baroutian S, Sarmah A (2018) Physicochemical, structural and combustion characterization of food waste hydrochar obtained by hydrothermal carbonization. Bioresour Technol 266:357–363. https://doi.org/10.1016/j.biortech.2018.06.112
Sekar M, Mathimani T, Alagumalai A, Chi NTL, Duc PA, Bhatia SK, Brindhadevi K, Pugazhendhi A (2021) A review on the pyrolysis of algal biomass for biochar and bio-oil—bottlenecks and scope. Fuel. https://doi.org/10.1016/j.fuel.2020.119190
Sevilla M, Fuertes AB (2009) The production of carbon materials by hydrothermal carbonization of cellulose. Carbon 47(9):2281–2289. https://doi.org/10.1016/j.carbon.2009.04.026
Shaheen S, Niazi N, Hassan N, Bibi I, Wang H, Tsang DCW, Ok YS, Bolan N, Rinklebe J (2019) Wood-based biochar for the removal of potentially toxic elements in water and wastewater: a critical review. Int Mater Rev 64(4):216–247. https://doi.org/10.1080/09506608.2018.1473096
Sharma K, Dutta V, Sharma S, Raizada P, Hosseini-Bandegharaei A, Thakur P, Singh P (2019) Recent advances in enhanced photocatalytic activity of bismuth oxyhalides for efficient photocatalysis of organic pollutants in water: a review. J Ind Eng Chem 78:1–20. https://doi.org/10.1016/j.jiec.2019.06.022
Shi HH, Wang MJ, Wang BB, Huang QG, Gao SX (2020) Insights on photochemical activities of organic components and minerals in dissolved state biochar in the degradation of atorvastatin in aqueous solution. J Hazard Mater. https://doi.org/10.1016/j.jhazmat.2020.122277
Silvestri S, Goncalves M (2019) TiO_2 supported on Salvinia molesta biochar for heterogeneous photocatalytic degradation of Acid Orange 7 dye. J Environ Chem Eng. https://doi.org/10.1016/j.jece.2019.102879
Sun J, He F, Pan Y, Zhang ZH (2017) Effects of pyrolysis temperature and residence time on physicochemical properties of different biochar types. Acta Agriculturae Scandinavica 67(1):12–22. https://doi.org/10.1080/09064710.2016.1214745
Sun F, Qu Z, Gao J, Wu HB, Liu F, Han R, Wang L, Pei T, Zhao G, Lu Y (2018) In situ doping boron atoms into porous carbon nanoparticles with increased oxygen graft enhances both affinity and durability toward electrolyte for greatly improved supercapacitive performance. Adv Funct Mater. https://doi.org/10.1002/adfm.201804190
Suo F, You X, Ma Y, Li Y (2019) Rapid removal of triazine pesticides by P doped biochar and the adsorption mechanism. Chemosphere 235:918–925. https://doi.org/10.1016/j.chemosphere.2019.06.158
Suresh AK, Pelletier DA, Doktycz MJ (2013) Relating nanomaterial properties and microbial toxicity. Nanoscale 5(2):463–474. https://doi.org/10.1039/c2nr32447d
Taba L, Irfan M, Daud W, Chakrabarti MH (2012) The effect of temperature on various parameters in coal, biomass and CO-gasification: a review. Renew Sustain Energy Rev 16(8):5584–5596. https://doi.org/10.1016/j.rser.2012.06.015
Tam M, Song J, Deb A, Cha L, Srivastava V, Sillanpaa M (2020) Biochar based catalysts for the abatement of emerging pollutants: a review. Chem Eng J 394:124856. https://doi.org/10.1016/j.cej.2020.124856
Tay H, Kajitani S, Zhang S, Li CZ (2013) Effects of gasifying agent on the evolution of char structure during the gasification of Victorian brown coal. Fuel 103:22–28. https://doi.org/10.1016/j.fuel.2011.02.044
Thiruppathi M, Leeladevi K, Ramalingan C, Chen KC, Nagarajan ER (2020) Construction of novel biochar supported copper tungstate nanocomposites: a fruitful divergent catalyst for photocatalysis and electrocatalysis. Mater Sci Semicond Process 106:10. https://doi.org/10.1016/j.mssp.2019.104766
Tomczyk A, Sokolowska Z, Boguta P (2020) Biochar physicochemical properties: pyrolysis temperature and feedstock kind effects. Rev Env Sci Biotechnol 19(1):191–215. https://doi.org/10.1007/s11157-020-09523-3
Vassilev SV, Baxter D, Andersen LK, Vassileva CG (2010) An overview of the chemical composition of biomass. Fuel 89(5):913–933. https://doi.org/10.1016/j.fuel.2009.10.022
Vithanage M, Seneviratne M, Ahmad M, Sarkar B, Ok YS (2017) Contrasting effects of engineered carbon nanotubes on plants: a review. Environ Geochem Health 39(6):1421–1439. https://doi.org/10.1007/s10653-017-9957-y
Wan Z, Sun Y, Tsang DCW, Hou D, Cao X, Zhang S, Gao B, Ok YS (2020) Sustainable remediation with an electroactive biochar system: mechanisms and perspectives. Green Chem 22(9):2688–2711. https://doi.org/10.1039/d0gc00717j
Wan Z, Xu Z, Sun Y, Zhang Q, Hou D, Gao B, Khan E, Graham NJD, Tsang DCW (2022) Stoichiometric carbocatalysis via epoxide-like C-S-O configuration on sulfur-doped biochar for environmental remediation. J Hazard Mater. https://doi.org/10.1016/j.jhazmat.2022.128223
Wang N, Ma WJ, Ren ZQ, Du YC, Xu P, Han XJ (2018a) Prussian blue analogues derived porous nitrogen-doped carbon microspheres as high-performance metal-free peroxymonosulfate activators for non-radical-dominated degradation of organic pollutants. J Mater Chem A 6(3):884–895. https://doi.org/10.1039/c7ta08472b
Wang T, Liu XQ, Ma CC, Liu Y, Dong HJ, Ma W, Liu Z, Wei MB, Li CX, Yan YS (2018b) A two step hydrothermal process to prepare carbon spheres from bamboo for construction of core-shell non-metallic photocatalysts. New J Chem 42(8):6515–6524. https://doi.org/10.1039/c8nj00953h
Wang T, Zhai Y, Zhu Y, Li C, Zeng G (2018c) A review of the hydrothermal carbonization of biomass waste for hydrochar formation: process conditions, fundamentals, and physicochemical properties. Renew Sustain Energy Rev 90:223–247. https://doi.org/10.1016/j.rser.2018.03.071
Wang WL, Wu QY, Huang N, Xu ZB, Lee MY, Hu HY (2018d) Potential risks from UV/H_2O_2 oxidation and UV photocatalysis: a review of toxic, assimilable, and sensory-unpleasant transformation products. Water Res 141:109–125. https://doi.org/10.1016/j.watres.2018.05.005
Wang XY, Lian WT, Sun X, Ma J, Ning P (2018e) Immobilization of NZVI in polydopamine surface-modified biochar for adsorption and degradation of tetracycline in aqueous solution. Front Environ Sci Eng. https://doi.org/10.1007/s11783-018-1066-3
Wang R, Huang D, Liu Y, Zhang C, Lai C, Wang X, Zeng GM, Gong XM, Duan A, Zhang Q, Xu P (2019a) Recent advances in biochar-based catalysts: properties, applications and mechanisms for pollution remediation. Chem Eng J 371:380–403. https://doi.org/10.1016/j.cej.2019.04.071
Wang T, Liu XQ, Men QY, Ma CC, Liu Y, Ma W, Liu Z, Wei MB, Li CX, Yan YS (2019b) Surface plasmon resonance effect of Ag nanoparticles for improving the photocatalytic performance of biochar quantum-dot/

$Bi_4Ti_3O_{12}$ nanosheets. Chinese J Catal 40(6):886–894. https://doi.org/10.1016/s1872-2067(19)63330-9
Wang Z, Sun P, Li Y, Meng T, Li Z, Zhang X, Zhang R, Jia H, Yao H (2019c) Reactive nitrogen species mediated degradation of estrogenic disrupting chemicals by biochar/monochloramine in buffered water and synthetic hydrolyzed urine. Environ Sci Technol 53(21):12688–12696. https://doi.org/10.1021/acs.est.9b04704
Wang CQ, Wang WL, Lin LT, Zhang FS, Zhang RN, Sun J, Song ZL, Mao YP, Zhao XQ (2020a) A stepwise microwave synergistic pyrolysis approach to produce sludge-based biochars: feasibility study simulated by laboratory experiments. Fuel. https://doi.org/10.1016/j.fuel.2020.117628
Wang H, Guo W, Liu B, Si Q, Luo H, Zhao Q, Ren N (2020b) Sludge-derived biochar as efficient persulfate activators: Sulfurization-induced electronic structure modulation and disparate nonradical mechanisms. Appl Catal B. https://doi.org/10.1016/j.apcatb.2020.119361
Wang TY, Liu SX, Mao W, Bai YC, Chiang K, Shah K, Paz-Ferreiro J (2020c) Novel Bi_2WO_6 loaded N-biochar composites with enhanced photocatalytic degradation of rhodamine B and Cr(VI). J Hazard Mater 389:11. https://doi.org/10.1016/j.jhazmat.2019.121827
Wang W, Wang H, Li G, Wong PK, An T (2020d) Visible light activation of persulfate by magnetic hydrochar for bacterial inactivation: efficiency, recyclability and mechanisms. Water Res 176:115746. https://doi.org/10.1016/j.watres.2020.115746
Wang YX, Rao L, Wang PF, Shi ZY, Zhang LX (2020e) Photocatalytic activity of N-TiO_2/O-doped N vacancy g-C_3N_4 and the intermediates toxicity evaluation under tetracycline hydrochloride and Cr(VI) coexistence environment. Appl Catal B. https://doi.org/10.1016/j.apcatb.2019.118308
Wang J, Cai J, Wang S, Zhou X, Ding X, Ali J, Zheng L, Wang S, Yang L, Xi S, Wang M, Chen Z (2022) Biochar-based activation of peroxide: Multivariate-controlled performance, modulatory surface reactive sites and tunable oxidative species. Chem Eng J. https://doi.org/10.1016/j.cej.2021.131233
Weber K, Quicker P (2018) Properties of biochar. Fuel 217:240–261. https://doi.org/10.1016/j.fuel.2017.12.054
Wen JQ, Xie J, Chen XB, Li X (2017) A review on g-C_3N_4-based photocatalysts. Appl Surf Sci 391:72–123. https://doi.org/10.1016/j.apsusc.2016.07.030
Wen E, Yang X, Chen H, Shaheen SM, Sarkar B, Xu S, Song H, Liang Y, Rinklebe J, Hou D, Li Y, Wu F, Pohorely M, Wong JWC, Wang H (2021) Iron-modified biochar and water management regime-induced changes in plant growth, enzyme activities, and phytoavailability of arsenic, cadmium and lead in a paddy soil. J Hazard Mater. https://doi.org/10.1016/j.jhazmat.2020.124344
Wu P, Wang Z, Bolan NS, Wang H, Wang Y, Chen W (2021) Visualizing the development trend and research frontiers of biochar in 2020: a scientometric perspective. Biochar 3(4):419–436. https://doi.org/10.1007/s42773-021-00120-3
Xia X, Zhu F, Li J, Yang H, Wei L, Li Q, Jiang J, Zhang G, Zhao Q (2020) A review study on sulfate-radical-based advanced oxidation processes for domestic/industrial wastewater treatment: degradation, efficiency, and mechanism. Front Chem. https://doi.org/10.3389/fchem.2020.592056
Xiang W, Zhang X, Chen J, Zou W, He F, Hu X, Tsang DCW, Ok YS, Gao B (2020) Biochar technology in wastewater treatment: a critical review. Chemosphere. https://doi.org/10.1016/j.chemosphere.2020.126539
Xie T, Reddy KR, Wang C, Yargicoglu E, Spokas K (2015) Characteristics and applications of biochar for environmental remediation: a review. Crit Rev Environ Sci Technol 45(9):939–969. https://doi.org/10.1080/10643389.2014.924180
Xie X, Li S, Zhang H, Wang Z, Huang H (2019) Promoting charge separation of biochar-based Zn-TiO_2/pBC in the presence of ZnO for efficient sulfamethoxazole photodegradation under visible light irradiation. Sci Total Environ 659:529–539. https://doi.org/10.1016/j.scitotenv.2018.12.401
Xu HD, Zhang YC, Li JJ, Hao QQ, Li X, Liu FH (2020) Heterogeneous activation of peroxymonosulfate by a biochar-supported Co_3O_4 composite for efficient degradation of chloramphenicols. Environ Pollut. https://doi.org/10.1016/j.envpol.2019.113610
Xu Z, Wan Z, Sun Y, Gao B, Hou DY, Cao XD, Komarek M, Ok YS, Tsang DCW (2022) Electroactive Fe-biochar for redox-related remediation of arsenic and chromium: distinct redox nature with varying iron/carbon speciation. J Hazard Mater. https://doi.org/10.1016/j.jhazmat.2022.128479
Yang Z, Wang Z, Liang G, Zhang X, Xie X (2021a) Catalyst bridging-mediated electron transfer for nonradical degradation of bisphenol A via natural manganese ore-cornstalk biochar composite activated peroxymonosulfate. Chem Eng J. https://doi.org/10.1016/j.cej.2021.131777
Yang ZS, Zhu P, Yan CM, Wang DAZ, Fang D, Zhou LX (2021b) Biosynthesized Schwertmannite@Biochar composite as a heterogeneous Fenton-like catalyst for the degradation of sulfanilamide antibiotics. Chemosphere. https://doi.org/10.1016/j.chemosphere.2020.129175
Yang X, Liu Z, Zhang J, Zheng J, Chen J, Liu Q, Li X, Wang Q, Li S, Ye Y, Wang D, Xie W, Liu J, Lan H, Wang J, Wang D, Zheng Z (2022) Boosting production of useful chemicals and micro-mesopores biochar from in situ catalytic pyrolysis of cellulose with red mud. Biomass Convers Biorefin. https://doi.org/10.1007/s13399-022-02778-6
Yao Z, Ma X, Lin Y (2016) Effects of hydrothermal treatment temperature and residence time on characteristics and combustion behaviors of green waste. Appl Therm Eng 104:678–686. https://doi.org/10.1016/j.applthermaleng.2016.05.111
Ye S, Yan M, Tan X, Liang J, Zeng G, Wu H, Song B, Zhou C, Yang Y, Wang H (2019) Facile assembled biochar-based nanocomposite with improved graphitization for efficient photocatalytic activity driven by visible light. Appl Catal B 250:78–88. https://doi.org/10.1016/j.apcatb.2019.03.004
Yi YQ, Tu GQ, Tsang PE, Fang ZQ (2020) Insight into the influence of pyrolysis temperature on Fenton-like catalytic performance of magnetic biochar. Chem Eng J 380:10. https://doi.org/10.1016/j.cej.2019.122518
Yu JF, Tang L, Pang Y, Zeng GM, Wang JJ, Deng YC, Liu YN, Feng HP, Chen S, Ren XY (2019) Magnetic nitrogen-doped sludge-derived biochar catalysts for persulfate activation: Internal electron transfer mechanism. Chem Eng J 364:146–159. https://doi.org/10.1016/j.cej.2019.01.163
Yu J, Feng H, Tang L, Pang Y, Zeng G, Lu Y, Dong H, Wang J, Liu Y, Feng C, Wang J, Peng B, Ye S (2020) Metal-free carbon materials for persulfate-based advanced oxidation process: microstructure, property and tailoring. Prog Mater Sci. https://doi.org/10.1016/j.pmatsci.2020.100654
Yun E, Lee J, Kim J, Park HD, Lee J (2018) Identifying the nonradical mechanism in the peroxymonosulfate activation process: singlet oxygenation versus mediated electron transfer. Environ Sci Technol 52(12):7032–7042. https://doi.org/10.1021/acs.est.8b00959
Zhai YL, Dai YZ, Guo J, Zhou LL, Chen MX, Yang HT, Peng LP (2020) Novel biochar@$CoFe_2O_4$/Ag_3PO_4 photocatalysts for highly efficient degradation of bisphenol a under visible-light irradiation. J Colloid Interface Sci 560:111–121. https://doi.org/10.1016/j.jcis.2019.08.065
Zhang SC, Lu XJ (2018) Treatment of wastewater containing Reactive Brilliant Blue KN-R using TiO_2/BC composite as heterogeneous photocatalyst and adsorbent. Chemosphere 206:777–783. https://doi.org/10.1016/j.chemosphere.2018.05.073
Zhang HY, Wang ZW, Li RN, Guo JL, Li Y, Zhu JM, Xie XY (2017) TiO_2 supported on reed straw biochar as an adsorptive and photocatalytic composite for the efficient degradation of sulfamethoxazole in aqueous matrices. Chemosphere 185:351–360. https://doi.org/10.1016/j.chemosphere.2017.07.025
Zhang J, Guo WL, Li QQ, Wang Z, Liu SJ (2018) The effects and the potential mechanism of environmental transformation of metal nanoparticles on their toxicity in organisms. Environ Sci Nano. https://doi.org/10.1039/c8en00688a
Zhang P, Shao YF, Xu XJ, Huang P, Sun HW (2020a) Phototransformation of biochar-derived dissolved organic matter and the effects on photodegradation of imidacloprid in aqueous solution under ultraviolet light. Sci Total Environ. https://doi.org/10.1016/j.scitotenv.2020.137913
Zhang S, Pi M, Su Y, Xu D, Xiong Y, Zhang H (2020b) Physiochemical properties and pyrolysis behavior evaluations of hydrochar from co-hydrothermal treatment of rice straw and sewage sludge. Biomass Bioenergy. https://doi.org/10.1016/j.biombioe.2020.105664
Zhang S, Wang J, Zhu S, Liu X, Xiong Y, Zhang H (2020c) Effects of $MgCl_2$ and $Mg(NO_3)_2$ loading on catalytic pyrolysis of sawdust for bio-oil and MgO-impregnated biochar production. J Anal Appl Pyrolysis. https://doi.org/10.1016/j.jaap.2020.104962
Zhang Y, Fan S, Liu T, Fu W, Li B (2022) A review of biochar prepared by microwave-assisted pyrolysis of organic wastes. Sustain Energy Techn. https://doi.org/10.1016/j.seta.2021.101873

Zhao B, O'Connor D, Zhang J, Peng T, Shen Z, Tsang DCW, Hou D (2018) Effect of pyrolysis temperature, heating rate, and residence time on rapeseed stem derived biochar. J Clean Prod 174:977–987. https://doi.org/10.1016/j.jclepro.2017.11.013

Zheng Y, Wang F, Yang X, Huang Y, Liu C, Zheng Z, Gu J (2017) Study on aromatics production via the catalytic pyrolysis vapor upgrading of biomass using metal-loaded modified H-ZSM-5. J Anal Appl Pyrolysis 126:169–179. https://doi.org/10.1016/j.jaap.2017.06.011

Zhou S, Liang H, Han L, Huang G, Yang Z (2019) The influence of manure feedstock, slow pyrolysis, and hydrothermal temperature on manure thermochemical and combustion properties. Waste Manag 88:85–95. https://doi.org/10.1016/j.wasman.2019.03.025

Zhou M, Xu Y, Luo G, Zhang Q, Du L, Cui X, Li Z (2022a) Facile synthesis of phosphorus-doped porous biochars for efficient removal of elemental mercury from coal combustion flue gas. Chem Eng J. https://doi.org/10.1016/j.cej.2021.134440

Zhou X, Liu X, Qi F, Shi H, Zhang Y, Ma P (2022b) Efficient preparation of P-doped carbon with ultra-high mesoporous ratio from furfural residue for dye removal. Sep Purif Technol. https://doi.org/10.1016/j.seppur.2022.120954

Zhu X, Liu Y, Qian F, Zhou C, Zhang S, Chen J (2015) Role of hydrochar properties on the porosity of hydrochar-based porous carbon for their sustainable application. ACS Sustain Chem Eng 3(5):833–840. https://doi.org/10.1021/acssuschemeng.5b00153

Zhu SS, Huang XC, Ma F, Wang L, Duan XG, Wang SB (2018) Catalytic removal of aqueous contaminants on N-doped graphitic biochars: inherent roles of adsorption and nonradical mechanisms. Environ Sci Technol 52(15):8649–8658. https://doi.org/10.1021/acs.est.8b01817

Zhuang Y, Kong Y, Liu Q, Shi B (2017) Alcohol-assisted self-assembled 3D hierarchical iron (hydr)oxide nanostructures for water treatment. CrystEngComm 19(39):5926–5933. https://doi.org/10.1039/c7ce01320e

Zhuang Y, Han B, Chen R, Shi B (2019) Structural transformation and potential toxicity of iron-based deposits in drinking water distribution systems. Water Res. https://doi.org/10.1016/j.watres.2019.114999